THE ASTROPHYSICAL JOURNAL, 545:309–326, 2000 December 10

CHEMISTRY OF THE ORGANIC-RICH HOT CORE G327.3−0.6

E. GIBB[1] AND A. NUMMELIN[1]
Department of Physics, Applied Physics and Astronomy, Rensselaer Polytechnic Institute, Troy, NY 12180
W. M. IRVINE
Five College Radio Astronomy Observatory, 619 Lederle Graduate Research Center, University of Massachusetts, Amherst, MA 01003
D. C. B. WHITTET[1]
Department of Physics, Applied Physics and Astronomy, Rensselaer Polytechnic Institute, Troy, NY 12180
AND
P. BERGMAN
Onsala Space Observatory, SE-439 92 Onsala, Sweden
Received 2000 May 22; accepted 2000 July 6

ABSTRACT

We present gas-phase abundances of species found in the organic-rich hot core G327.3−0.6. The data were taken with the Swedish-ESO Submillimetre Telescope (SEST). The 1–3 mm spectrum of this source is dominated by emission features of nitrile species and saturated organics, with abundances greater than those found in many other hot cores, including Sgr B2 and OMC-1. Population diagram analysis indicates that many species (CH_3CN, C_2H_3CN, C_2H_5CN, CH_3OH, etc.) have hot components that originate in a compact ($\sim 2''$) region. Gas-phase chemical models cannot reproduce the high abundances of these molecules found in hot cores, and we suggest that they originate from processing and evaporation of icy grain mantle material. In addition, we report the first detection of vibrationally excited ethyl cyanide and the first detection of methyl mercaptan (CH_3SH) outside the Galactic center.

Subject headings: ISM: abundances — ISM: individual (G327.3−0.6) — ISM: molecules — line: identification — radio lines: ISM

1. INTRODUCTION

1.1. *General*

Hot cores are compact, warm ($\sim$100–300 K), dense ($\sim 10^7$ H nuclei cm^{-3}) clouds of gas and dust associated with recent high-mass star formation. The hot-core phase is thought to last about 10^5 yr (van Dishoeck & Blake 1998) and represents the most chemically rich phase of the interstellar medium. The complex chemical and physical processes occurring in these regions are not well understood. To date, the chemistry of few hot cores has been studied in detail. Those that have been include the cores within Sgr B2 (Turner 1991; Nummelin et al. 1998a), OMC-1 (Blake et al. 1987; Sutton et al. 1995), G34.3+0.15 (Macdonald et al. 1996), and W3 (Helmich & van Dishoeck 1997). There appear to be significant differences in physical and chemical conditions among these hot cores. A high abundance of complex saturated organic molecules could indicate evaporation of molecules processed on dust grains. Varying abundances of sulfur-bearing species could be an indication of evolutionary state (Charnley 1997; Hatchell et al. 1998). More sources need to be added to the inventory of studied hot cores before their chemical evolution can be understood.

The composition of the gas in hot cores is intimately related to the composition of dust grains. These dust grains consist of a refractory core covered by a volatile icy mantle that forms as gaseous molecules and atoms collide and stick to the refractory core in the cold, protected dark clouds. The ice composition may be modified by processes on or in the mantles themselves, and material may be released back into the gas phase by radiative heating, starting with the most volatile molecules (Ehrenfreund et al. 1998). Subsequent high-temperature reactions in the gas phase among the sublimated molecules and the preexisting gas species result in a very rich chemistry (Charnley, Tielens, & Millar 1992; Caselli, Hasegawa, & Herbst 1993). Infrared observations are sensitive enough to detect molecules with an abundance $\sim$1% that of water. Millimeter observations can detect molecules with abundances $\sim 10^{-11}$ that of H_2. Assuming an average water abundance in hot cores of $\sim 10^{-5}$ that of H_2 (Gensheimer, Mauersberger, & Wilson 1996), it is obvious that the greater sensitivity of millimeter observations allows an opportunity to indirectly study trace constituents of grain mantles that are otherwise undetectable.

Studies of icy mantles in dark clouds have been greatly aided by the recent *Infrared Space Observatory* (*ISO*) mission. The mantles themselves consist of two distinct phases. The first is a polar (H_2O-rich) layer, which may be covered by the second phase, a nonpolar (CO-rich) mantle. Thus far, detected molecules in the icy mantle include H_2O, CO_2, CO, OCS, CH_3OH, CH_4, NH_3, organics, and "XCN," a feature that is due to the C≡N stretch mode of a species that has not yet been firmly identified. The simplest species are modified by a combination of surface reactions and/or processing by UV photons, cosmic rays, X-rays, and thermal polymerization. Laboratory UV irradiation experiments show a variety of formation products. Polar mixtures composed of H_2O, CH_3OH, and traces of NH_3 yield H_2CO, CH_4, CO_2, moderately complex organic molecules, and CN-bearing species (Bernstein et al. 1995; Sandford, Allamandola, & Bernstein 1997). Nonpolar mixtures composed of N_2, O_2, CO, and CO_2 produce such molecules as CO_2, N_2O, O_3, and CO_3 (Sandford et al. 1997). Warming of

[1] New York Center for Studies on the Origins of Life, Rensselaer Polytechnic Institute, Troy, NY 12180.

these ices results in sublimation of the most volatile, such as CO, N_2, and O_2, and allows neighboring reactive species to interact to form new complex molecules such as ethanol, formamide, and acetamide (Bernstein et al. 1995). The warming that occurs in the formation of hot cores will evaporate most of the mantle molecules to the gas phase to drive the complex gas-phase chemistry referred to above, before the cloud is eventually dispersed by stellar winds.

1.2. *G327.3−0.6*

We have studied the hot-core position in the southern molecular cloud G327.3−0.6 (hereafter G327; R.A.(1950) = $15^h49^m15^s.6$, decl.(1950) = −54°28′07″), located at a kinematical distance of 2.9 kpc (Simpson & Rubin 1990). Both OH and H_2O masers indicate recent or ongoing massive star formation. Bergman (1992) analyzed CH_3CN and CH_3CCH maps of G327 and determined the presence of two molecular cores separated by 60″, or 0.8 pc. One is cold ($T_k \approx 30$ K) and the other hot ($T_k \approx 150$ K). The physical characteristics of the latter are shown in Figure 1. Our data show the existence of a dense, hot core that is extremely rich in emission lines at millimeter wavelengths, making this source excellent for astrochemical studies. The lines are also relatively symmetric, Gaussian in shape, and narrower (~ 5 km s^{-1}) than in sources such as Sgr B2 ($\sim$15–20 km s^{-1}; Nummelin et al. 2000), so that blending and line confusion is much less of a problem. This paper is based on data collected during ground-based millimeter-wave searches for several complex organic molecules (see § 2.1).

Observed millimeter continuum flux densities and the rich molecular spectrum detected toward G327 support the presence of an ultracompact H II region. The FWHM size of the hot-core region determined by Bergman (1992) using a homogeneous large velocity gradient (LVG) model based on emission from vibrationally excited CH_3CN is 7×10^{16} cm (0.02 pc) in diameter and is within the range expected for ultracompact H II regions (Wood & Churchwell 1989). The kinetic temperature seems to be high throughout the compact region. Since $T_k < T_d$ in the hot IR region, the molecular gas is probably thermally decoupled from the dust. Under the assumption that the $^{12}C^{18}O$ emission is optically thin and fills the beam, Bergman (1992) estimated the mass of the ultracompact core in his three-component model to be of the order of 20 $M_\odot$ with $T_k = 150$–200 K. The outer hot core is somewhat cooler with a diameter of 2×10^{17} cm. This is surrounded by a cool (40–60 K) envelope. A range of hydrogen densities in each region was determined by Bergman (1992) (see Fig. 1) and the implications are discussed in § 6.

The *Infrared Space Observatory* (*ISO*) also observed G327 with both its Short Wavelength Spectrometer (SWS) and Long Wavelength Spectrometer (LWS). The spectrum is dominated by polycyclic aromatic hydrocarbon (PAH) emission and ionized metal lines. Using the ratio of the S III lines at 33 and 19 μm and the O III lines at 88 and 52 μm, Ehrenfreund et al. (1997) estimated the effective temperature of the star illuminating the H II region to be 36,000–40,000 K.

2. OBSERVATIONS AND DATA REDUCTION

2.1. *Observations*

The millimeter observations used in this study were taken during the course of four observing runs at the 15 m Swedish-ESO Submillimetre Telescope[2] (SEST; Booth et al. 1989) at La Silla, Chile, in 1998 June, 1997 October, 1998 October, and 1999 October. We used the SESIS 100/150 GHz and the IRAM 115/230 GHz SIS receivers to obtain

[2] The Swedish-ESO Submillimetre Telescope is operated jointly by ESO and the Swedish National Facility for Radio Astronomy, Onsala Space Observatory, at Chalmers University of Technology.

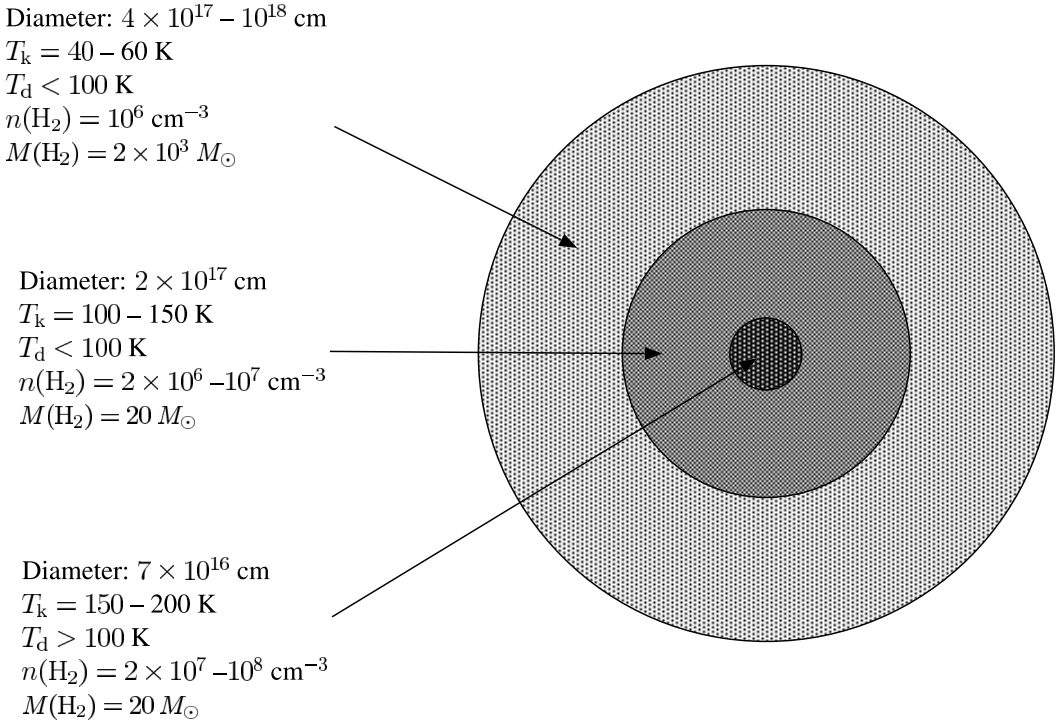

FIG. 1.—Physical structure of the hot core in G327.3−0.6, as derived by Bergman (1992) based on modeling of the CH_3CN and CH_3CCH emission

spectra of several hot cores as part of a search for ethylene oxide (c-C_2H_4O; Nummelin et al. 1998b), vinyl alcohol (CH_2CHOH), cyclopropenone (c-HCCOCH), and furan (c-C_3H_4O; Dickens et al. 2000). The system was calibrated using the standard chopper wheel method (Kutner & Ulich 1981).

System temperatures in the 1997 October observing run were ~200 K at 3 mm up to 500 K at 1 mm. In 1998 October, they were ~200 K for 2 mm to ~425 K for 1 mm. Pointing was checked regularly using the SiO masers VX Sgr or IRSV 1540. All observations were performed in dual beam switching mode with a beam separation of 12′ on the sky, producing flat spectral baselines. A spectrometer bandwidth of about 1 GHz and 1440 channels provided a resolution of 1.4 MHz. We assumed an emission velocity with respect to the local standard of rest, $V_{LSR} = -45.0$ km s^{-1}, for G327. Since weak lines were searched for during these observing runs, the resulting spectra have an exceptionally high signal-to-noise ratio with a noise rms of 5–25 mK (T_A^*). A sample spectrum is shown in Figure 2.

In 1999 October, maps of the $J = 12_{0,12} \rightarrow 11_{0,11}$ line at 105.47 GHz and the $J = 26 \rightarrow 25$ band around 233.2 GHz of ethyl cyanide were obtained in the dual receiver mode. The angular resolutions were 48″ and 22″, respectively, at these frequencies. A 90″ × 90″ area was sampled at 10″ spacing. Typical system temperatures were between 200 and 400 K. In order to minimize the effects of pointing variations within a map, short integration times (usually 60 s) and several reruns with pointing checks between the maps were used throughout the observing run. First- or second-order baselines were removed from the spectra during the data reduction.

The data were reduced and analyzed using the XS software package written by Per Bergman at Onsala Space Observatory.

2.2. *Line Identification*

We compared the frequencies of our detected lines with several catalogs of predicted and laboratory-measured frequencies. For most molecules, we used the catalogs compiled by Lovas (1985), Spectral Line Atlas of Interstellar Molecules (SLAIM; Lovas 1984), and the JPL molecular line catalog (Pickett et al. 1998). To be considered as a possible assignment, the lines in the catalogs had to be within ≈1.5 MHz of the measured line positions. These catalogs are incomplete for several molecules, and for these we used other laboratory studies. For methanol (CH_3OH) we used Anderson, Herbst, & De Lucia (1987); ^{13}C methanol ($^{13}CH_3OH$) transitions are from Anderson, De Lucia, & Herbst (1990); methyl formate (CH_3OCHO) lines were taken from a recent paper by Oesterling et al. (1999); lab assignments for dimethyl ether (CH_3OCH_3) were taken from Groner et al. (1998) and methyl mercaptan (CH_3SH) from Bettens et al. (1999). We eliminated from our analysis lines that were blended or that could be assigned to more than one likely molecule.

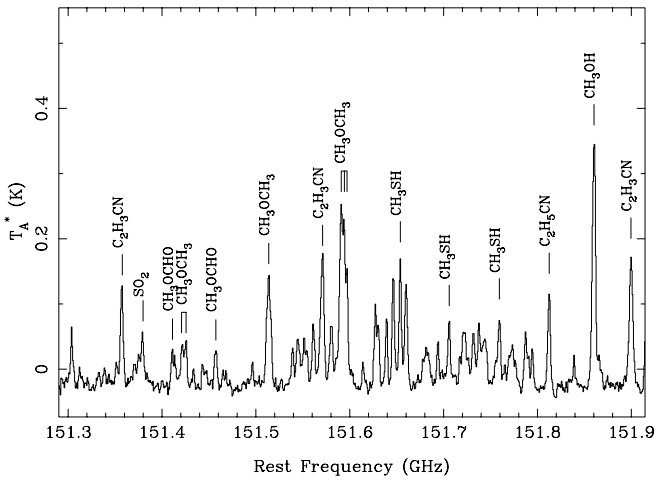

FIG. 2.—Sample spectrum around 151.6 GHz, with suggested line identifications marked. The majority of the emission lines are from asymmetric organic species such as CH_3OH, CH_3OCHO, C_2H_3CN, C_2H_5CN, and CH_3SH. Approximately one-half of the lines in this band—unmarked in the figure—are as yet unidentified.

3. DATA ANALYSIS

3.1. *The Population Diagram Method*

For molecular species with three or more detected transitions spanning a sufficiently large range of energies above the ground state, column densities and rotational temperatures were derived using the population diagram method outlined by Goldsmith & Langer (1999). In its simplest form it assumes that (1) the population of all molecular energy levels is in equilibrium at a certain temperature, referred to as the rotational temperature, T_{rot}, (2) the emission is optically thin (i.e., optical depth $\tau \ll 1$ and $1 - e^{-\tau} \approx \tau$), (3) the source is homogeneous and fills the antenna beam, and (4) the influence of the background radiation field can be neglected. Given these assumptions, it can be shown that

$$\ln\left(\frac{8\pi k \nu_{ul}^2}{hc^3 A_{ul} g_u} \int T_{mb}\, dV_{LSR}\right) = \ln\left(\frac{N_u}{g_u}\right) = \ln\left(\frac{N}{Z(T_{rot})}\right) - \frac{E_u}{kT_{rot}}, \quad (1)$$

where k and h are Boltzmann's and Planck's constants, respectively, c is the speed of light, ν_{ul} is the frequency of the transition $u \rightarrow l$, A_{ul} is the corresponding Einstein A-coefficient, g_u is the statistical weight of the upper level, T_{mb} is the main-beam brightness temperature, and V_{LSR} is the emission velocity with respect to the local standard of rest. E_u is the energy of the upper state, and N and N_u are the total column density and the column density in level u, respectively. By plotting the left-hand quantity of equation (1) against E_u for each observed line and fitting a straight line to the data, T_{rot} can be found as the negative inverse of the slope and $\ln(N/Z(T_{rot}))$, and thus also N, as the intercept of the y-axis.

The rotational partition function at temperature T_{rot}, $Z(T_{rot})$ is given by

$$Z(T_{rot}) = \sum_{i=0}^{\infty} g_i\, e^{-E_i/kT_{rot}}, \quad (2)$$

where $g_i = 2i + 1$ is the rotational statistical weight. For a linear molecule, the partition function was approximated by (Blake et al. 1987; Turner 1991)

$$Z_{lin}(T_{rot}) \approx \frac{kT_{rot}}{hB}. \quad (3)$$

TABLE 1

LOWER LIMITS ON THE COLUMN DENSITIES FOR SPECIES WITH ONE OR TWO DETECTED LINES

Species	ν(rest) (GHz)	E_u/k (K)	N (cm^{-2})	$N(x)/N(H_2)$[a]
$C^{17}O$	112.359	5	2.1(16)	6.6(−8)
NS	253.970	40	2.2(15)	6.9(−9)
SO	254.574	100	1.1(15)	3.4(−9)
SO	86.094	19	4.0(14)	1.3(−9)
^{34}SO	135.755	16	2.9(13)	9.1(−11)
^{34}SO	84.411	19	3.6(13)	1.1(−10)
$C^{34}S$	96.413	7	6.3(13)	2.0(−10)
$C^{34}S$	241.016	35	4.2(13)	1.3(−10)
OCS	97.301	21	6.0(14)	1.9(−9)
CCS	86.181	23	6.1(12)	1.9(−11)
CCS	93.870	20	6.8(12)	2.1(−11)
HDO	225.897	168	2.2(14)	6.9(−10)
c–SiCC	93.064	11	2.4(12)	7.4(−12)
c–SiCC	94.245	19	3.1(12)	9.6(−12)
SiO	217.105	31	8.7(12)	2.7(−11)
N_2H^+	93.174	5	1.6(14)	5.0(−10)
CH_2NH	225.554	11	1.3(13)	4.0(−11)
CH_2NH	250.161	97	1.0(14)	3.1(−10)
H_2CO	225.698	33	4.5(14)	1.4(−9)
H_2CO	101.333	83	2.2(15)	6.8(−9)
HNCO	240.876	113	5.1(13)	1.6(−10)
HC_3N	136.464	52	2.3(14)	7.2(−10)
HC_3N	254.700	177	7.8(13)	2.4(−10)
$HC^{13}CCN$	135.886	52	1.8(13)	5.6(−11)
$HCC^{13}CN$	135.898	52	3.5(13)	1.1(−10)
$H^{13}CN$	86.339	4	8.4(13)	2.6(−10)
$H^{13}CO^+$	86.754	4	8.6(12)	2.7(−11)

NOTE.—$a(b) = a \times 10^b$.

[a] Assuming $N(H_2) = 3.2(23)$.

Symmetric and asymmetric top molecules were approximated by

$$Z(T_{\rm rot}) \approx \sqrt{\frac{\pi}{ABC}\left(\frac{kT_{\rm rot}}{h}\right)^3}, \tag{4}$$

where A, B, and C are the rotational constants (in hertz) of the molecule such that $A > B > C$. In the case of symmetric top molecules, $A = B$. In addition, factors due to spin weights (e.g., ortho/para) were accounted for where appropriate. The approximations above are valid when $hB \ll kT$.

Two of the simplifying assumptions used to derive equation (1) may not be valid, complicating the analysis. The first is that the optical depths are not necessarily small for all molecules and transitions. As was shown by Goldsmith & Langer (1999), if a line is optically thick the intensity will be below its optically thin value by a factor equal to the inverse of the photon escape probability,

$$C_\tau = \frac{\tau}{1 - e^{-\tau}}, \tag{5}$$

and therefore, if the optical depth can be determined, the ordinate of the population diagrams can be corrected by adding an amount $\ln(C_\tau)$.

The second complication is that the discussion so far has assumed that the source fills the antenna beam. If the extent of the emitting gas does not completely fill the antenna pattern or if the source is clumpy, the observed antenna temperature has to be multiplied by the dilution factor ($\Delta\Omega_a/\Delta\Omega_s$), which is the ratio of the solid angle of the antenna beam to that subtended by the source. In the case of single-dish observations, the dilution factor may be large ($>10^2$) for hot-core emission, and, if not accounted for properly, this will lead to severely underestimated column densities and optical depths (Wyrowsky, Schilke, & Walmsley 1999; Nummelin et al. 2000; Schilke, Phillips, & Mehringer 1999).

Taking the finite optical depth and beam dilution into account, the modified relationship will then be

$$\ln\left(\frac{\gamma_u W}{g_u}\right) + \ln(C_\tau) + \ln\left(\frac{\Delta\Omega_a}{\Delta\Omega_s}\right) = \ln\left(\frac{N}{Z(T_{\rm rot})}\right) - \frac{E_u}{kT_{\rm rot}}, \tag{6}$$

where γ_u is the combination of constants relating integrated intensity and upper level column density given by

$$\gamma_u = \frac{8\pi k \nu_{ul}^2}{hc^3 A_{ul}} \tag{7}$$

and W is the integrated line intensity.

We find the set of free parameters $T_{\rm rot}$, N, and $\Delta\Omega_a/\Delta\Omega_s$ that best fitted the data to a straight line in the population diagram by trying all possible values of the free parameters and finding the combination that minimizes the χ^2-value. Assuming the gas is thermalized, the rotation temperature thus derived should be equal to the kinetic temperature. Care must be used in this interpretation. For instance, if the H_2 density is insufficient to thermalize some or all of the transitions, subthermal temperatures are deduced (Goldsmith & Langer 1999). Also, it is possible that the fitting procedure can give false minima for $T_{\rm rot}$ and N. For example, when the source size is left as a free parameter, the minimum χ^2 for C_2H_5OH (see § 4.1.3) occurs at a physically unreasonable temperature of 4 K and a column density exceeding that of H_2. In this case, we kept only the beam-filled fit, as the scatter in the data did not warrant a more detailed analysis.

For molecules with only one or two detections, we calculated a lower limit to the beam-averaged column density by using E_u/k for the rotation temperature, assuming negligible optical depth and setting $\Delta\Omega_a/\Delta\Omega_s = 1$. It can be shown (Hatchell et al. 1998) by setting the derivative of the temperature-dependent component of equation (1) equal to zero that the turning point of the temperature is $T_{\rm rot} = E_u/k$ for linear molecules and $T_{\rm rot} = 2E_u/3k$ for symmetric and asymmetric top molecules. Taking the second derivative shows that this is a minimum. These results are shown in Table 1.

4. RESULTS

4.1. *Rotation Temperatures, Column Densities, and Source Sizes*

The rotational temperatures and molecular column densities derived from the population diagram analysis are summarized in Tables 2 and 3 and the lower limits in Table 1. Table 2 shows the results under the assumption that the gas is extended beyond the size of the SEST beam. The population diagrams corresponding to this table are shown in Figure 3. Table 3 shows the data for the hot-core molecules for which high rotation temperatures and small

TABLE 2

BEAM-AVERAGED COLUMN DENSITIES

Molecule	Number of Lines	E_u/k (K)	T_{rot} (K)	N (cm^{-2})	$N(x)/N(H_2)$[a]
CH_3OH	25	19–692	180^{+14}_{-11}	$1.68(16)^{+0.1}_{-0.1}$	5.3(−8)
$^{13}CH_3OH$	20	7–307	93^{+11}_{-10}	$1.70(15)^{+0.2}_{-0.2}$	5.3(−9)
C_2H_5OH	13	13–229	66^{+11}_{-8}	$8.32(14)^{+0.8}_{-0.9}$	2.6(−9)
CH_3OCH_3	19	8–313	82^{+8}_{-7}	$1.15(17)^{+0.1}_{-0.1}$	3.4(−7)
CH_3OCHO	83	8–556	375^{+62}_{-50}	$1.62(16)^{+0.3}_{-0.2}$	5.0(−8)
CH_3CHO	11	15–93	45^{+10}_{-7}	$1.62(14)^{+0.3}_{-0.2}$	5.0(−10)
$HCOOH$	6	14–88	71^{+64}_{-22}	$8.51(13)^{+7.9}_{-2.5}$	2.7(−10)
CH_3CCH	5	86–201	72^{+29}_{-16}	$2.19(15)^{+0.4}_{-0.3}$	6.9(−9)
CH_3CN	11	80–942	952^{+612}_{-243}	$1.00(16)^{+3.0}_{-0.5}$	3.1(−8)
$CH_3^{13}CN$	5	114–658	252^{+78}_{-46}	$1.46(14)^{+0.6}_{-0.3}$	4.6(−10)
$^{13}CH_3CN$	9	25–440	282^{+125}_{-65}	$2.40(14)^{+2.5}_{-0.8}$	7.5(−10)
C_2H_3CN	37	22–575	303^{+39}_{-29}	$7.76(14)^{+2.0}_{-1.3}$	2.4(−9)
C_2H_5CN	85	14–614	208^{+11}_{-9}	$2.48(15)^{+0.2}_{-0.2}$	7.8(−9)
NH_2CHO	5	10–269	208^{+168}_{-63}	$1.01(14)^{+1.2}_{-0.4}$	3.1(−10)
OCS[b]	6	16–134	106^{+70}_{-22}	$7.27(15)^{+1.1}_{-0.3}$	2.3(−8)
H_2CS	5	23–164	53^{12}_{-8}	$3.98(14)^{+0.7}_{-0.6}$	1.2(−9)
SO_2	7	15–163	130^{+80}_{-34}	$7.41(14)^{+5.5}_{-2.0}$	2.3(−9)
CH_3SH	11	20–95	68^{+45}_{-19}	$1.17(15)^{+1.0}_{-0.3}$	3.7(−9)

NOTE.—$a(b) = a \times 10^b$.

[a] Assuming $N(H_2) = 3.2(23)$ (Bergman 1992).

[b] The fit was obtained using both isotopomers and assuming $[^{12}C]/[^{13}C] = 40$ and $[^{32}S]/[^{34}S] = 22$ for $[OC^{34}S]/[O^{13}CS] = 1.82$.

source sizes are deduced. Figure 4 shows the population diagrams for these species with the source size set to 2″, the average size determined for the hot-core molecules in Table 3. The following section outlines the results of the diagrams, with discussion and implications in § 6.

Population diagrams are shown for molecules with at least three detected transitions in Figures 3 and 4. The rotation temperatures and beam-averaged column densities are shown in Table 2. All errors are 1 σ errors derived from the boundaries of the 68% confidence regions

$$\chi_v^2 \leq \chi_{v,\,\min}^2 + \Delta\chi_v^2 , \tag{8}$$

where

$$\Delta\chi_v^2 = x/(N - P) \tag{9}$$

and where N is the number of data points, P is the number of fitted parameters (T_{rot}, N, θ_s), and x equals 1.0, 2.3, and

TABLE 3

COLUMN DENSITIES AND ABUNDANCES FOR HOT-CORE MOLECULES

			Free Source Size			2″ Source Size[a]		
Molecule	Number of Lines	E_u/k	T_{rot} (K)	N (cm^{-2})	Source Size (arcsec)	T_{rot} (K)	N (cm^{-2})	Abundance
CH_3OH[b]	28	60–692	102^{+10}_{-10}	$5.50(19)^{+3.2}_{-1.3}$	$2.38^{+0.18}_{-0.09}$	118^{+6}_{-8}	$6.03(19)^{+1.9}_{-1.0}$	2(−5)
CH_3OCH_3	19	8–313	50^{+16}_{-10}	$5.13(19)^{+2.3}_{-1.4}$	$6.29^{+1.10}_{-0.80}$			
CH_3OCHO	83	8–556	170^{+16}_{-18}	$5.13(17)^{+1.0}_{-1.2}$	$1.91^{+0.16}_{-0.09}$	162^{+11}_{-9}	$4.79(18)^{+0.3}_{-0.3}$	2(−6)
SO_2	7	15–163	112^{+78}_{-46}	$3.09(17)^{+3.3}_{-2.2}$	$2.24^{+1.00}_{-0.21}$	134^{+47}_{-28}	$4.68(17)^{+1.6}_{-1.1}$	2(−7)
HCN[c]	1	4				150	4.4(18)	1(−6)
$HNCO$[c]	1	113				150	9.2(15)	3(−9)
HC_3N[c]	1	177				150	8.0(13)	3(−11)
CH_3CN[b]	25	25–942	162^{+15}_{-14}	$1.74(18)^{+0.8}_{-0.3}$	$2.11^{+0.09}_{-0.20}$	164^{+12}_{-10}	$2.09(18)^{+0.2}_{-0.2}$	7(−7)
C_2H_3CN	37	22–575	131^{+15}_{-18}	$2.61(18)^{+1.0}_{-0.7}$	$1.39^{+0.08}_{-0.09}$			
C_2H_3CN (grnd)[d]	25	22–229	49^{+7}_{-9}	$3.16(17)^{+1.4}_{-0.9}$	$2.55^{+0.20}_{-0.18}$	69^{+5}_{-5}	$5.25(17)^{+1.8}_{-1.3}$	2(−7)
C_2H_3CN (vib)[d]	12	369–575	186^{+193}_{-112}	$4.37(18)^{+35.4}_{-2.1}$	$0.94^{+0.51}_{-0.14}$	225^{+47}_{-70}	$4.79(17)^{+2.0}_{-0.6}$	2(−7)
C_2H_5CN	85	14–614	138^{+7}_{-9}	$1.60(18)^{+0.4}_{-0.3}$	$1.85^{+0.11}_{-0.11}$	135^{+5}_{-5}	$1.27(18)^{+0.1}_{-0.1}$	4(−7)
NH_2CHO	5	10–269	72^{+32}_{-47}	$6.46(16)^{+530}_{-3.2}$	$2.01^{+1.19}_{-0.27}$	73^{+17}_{-14}	$6.31(16)^{+5.6}_{-1.8}$	2(−8)

NOTE.—$a(b) = a \times 10^b$.

[a] Assuming $N(H_2) = 3 \times 10^{24}$. See discussion in § 4.2.

[b] The fit was obtained simultaneously using both the ^{13}C and ^{12}C isotopomers and assuming $[^{12}C]/[^{13}C] = 40$.

[c] Estimated assuming an optically thin transition with $T_{rot} = 150$ K and $[^{12}C]/[^{13}C] = 40$ as outlined in § 4.1.1. Since HC_3N is a cold-gas tracer with a possible hot component, we used only the 177 K transition to estimate the hot-core component.

[d] The rotational and vibrationally excited lines for vinyl cyanide were treated separately, as they probably represent different physical components of the gas. See § 6.1.1 for details.

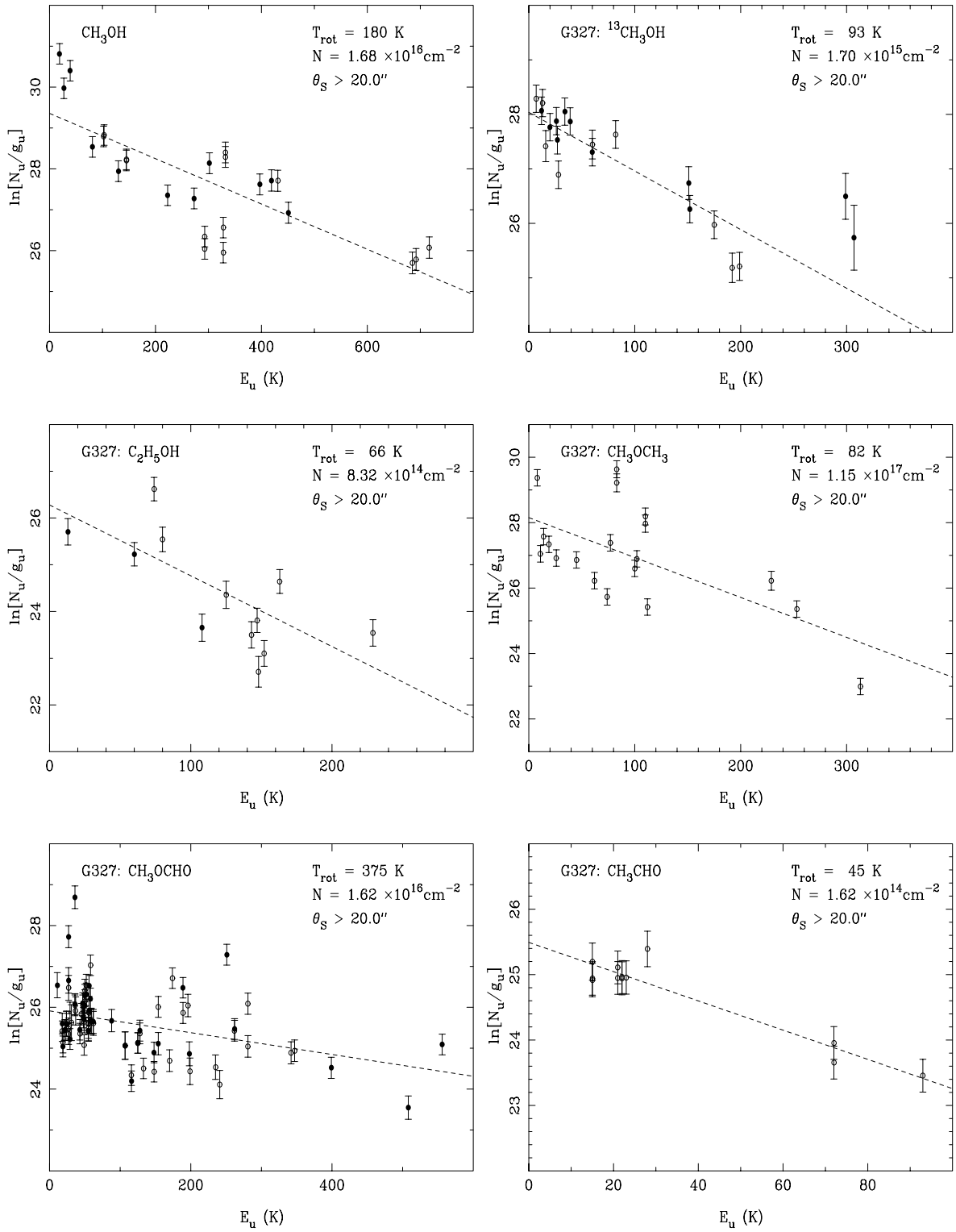

FIG. 3.—Population diagrams for molecules assuming extended (> 20″) emission. The filled/open circles in the CH_3OH, $^{13}CH_3OH$, C_2H_5OH, CH_3OCHO, and CH_3SH plots are for *E*/*A* transitions, respectively. The stars in the C_2H_3CN and C_2H_5CN panels correspond to the vibrationally excited transitions. The dotted line is the best-fit model. The error bars indicate the 30% pointing and calibration uncertainty.

3.5 for 1, 2, and 3 free parameters, respectively (Lampton, Margon, & Bowyer 1976).

4.1.1. *Nitriles*

Nitriles are one of the dominant sources of emission in our data. We have detections of isocyanic acid (HNCO), hydrogen cyanide ($H^{13}CN$), cyanoacetylene (HC_3N, $HC^{13}CCN$, $HCC^{13}CN$), methyl cyanide (CH_3CN, $CH_3{}^{13}CN$, $^{13}CH_3CN$), vinyl cyanide (C_2H_3CN), and ethyl cyanide (C_2H_5CN). Most of these molecules (the unsaturated HC_3N being an exception) are tracers of hot cores and are predicted to be strongly peaked toward a compact

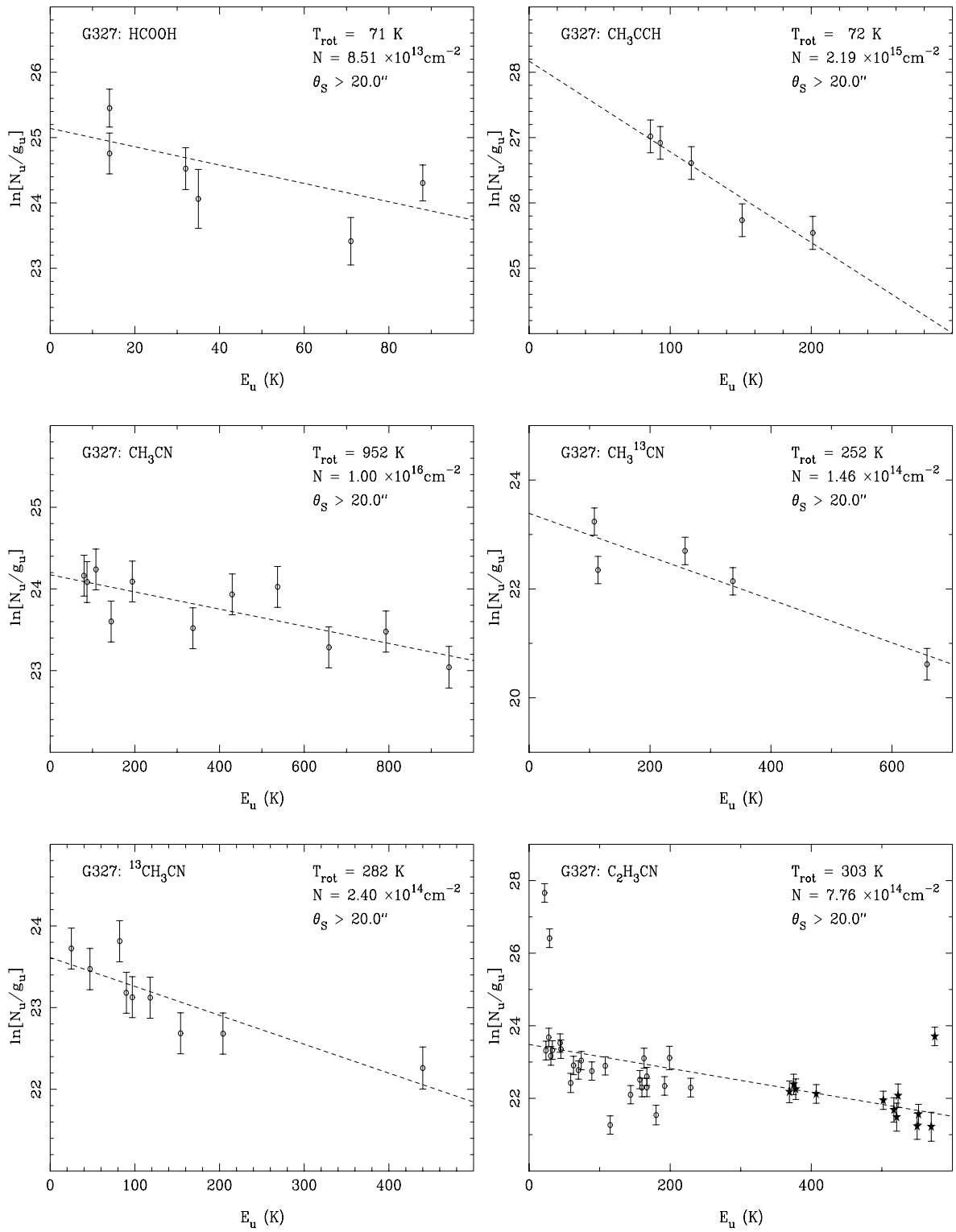

FIG. 3.—*Continued*

region with a large rotation temperature. This is supported by the 1.″4–2.″1 (0.02–0.03 pc) source sizes and 128–162 K temperatures derived from the population diagrams for CH_3CN, C_2H_3CN, and C_2H_5CN. In addition, energies above the ground state ranging from 14 to 614 K for C_2H_5CN, 22 to 575 K for C_2H_3CN, and 80 to 942 K for CH_3CN require a very hot gas component for excitation.

For HNCO, $H^{13}CN$, and HC_3N only lower limits on the column density were obtained, since not enough transitions were observed to define an accurate population diagram. If we assume that the lines are optically thin, the emission comes from a 2″ source, and the rotation temperature is similar to that for the other nitriles ($\sim$150 K), we deduce column densities of 9.2×10^{15} cm^{-2} and 1.1×10^{17} cm^{-2} for HNCO and $H^{13}CN$, respectively. We analyzed HC_3N and two of its ^{13}C isotopes ($HC^{13}CCN$ and $HCC^{13}CN$) by assuming a 2″ source size and $[^{12}C]/[^{13}C] = 40$ as determined by Bergman (1992) by comparing the column

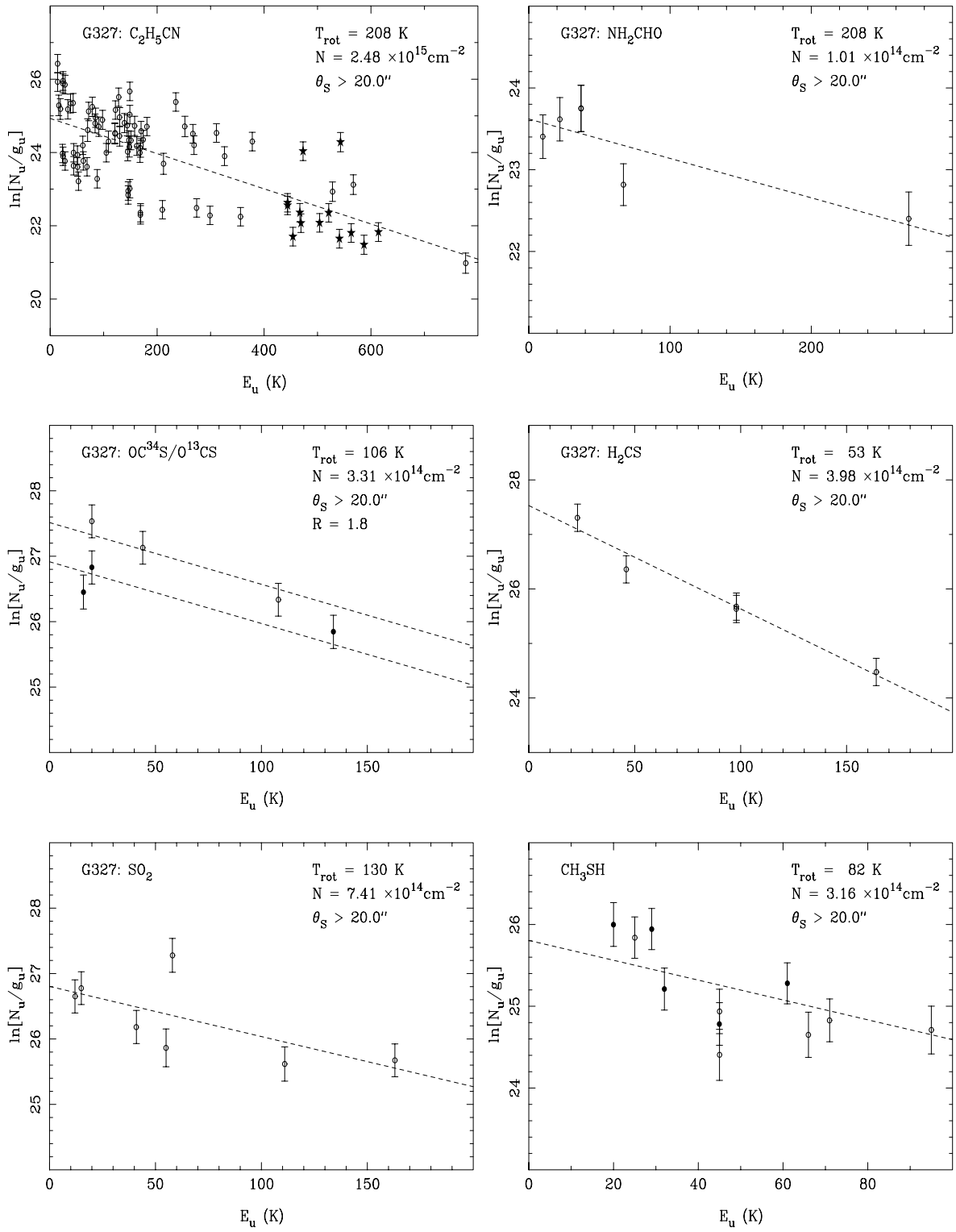

FIG. 3.—*Continued*

density ratio $N(C^{18}O)/N(^{13}C^{18}O)$ and compensating for a $^{12}C^{18}O$ ($J = 2 \rightarrow 0$) optical depth of ~ 0.5. This gives $N = 6.9 \times 10^{16}$ cm^{-2} and $T_{rot} = 155$ K, though the best fit is for a large source ($T_{rot} = 54$ K) and gives a column density of 7.9×10^{13} cm^{-2}, which is more consistent with its role as a tracer of cold gas.

The three isotopes of CH_3CN when analyzed separately give a wide range of temperatures, from 252 to 952 K for beam-averaged fits and 124 to 390 K for small source sizes (see Tables 2 and 3). The higher, poorly constrained temperature for the main isotope is likely due to insufficient opacity corrections for the optically thick low-energy transitions, which will also result in an underestimated column density. $^{13}CH_3CN$ and $CH_3^{13}CN$ give similar temperatures of ~ 150 K for compact source sizes. A rotational temperature of 150 K is also consistent with that derived using

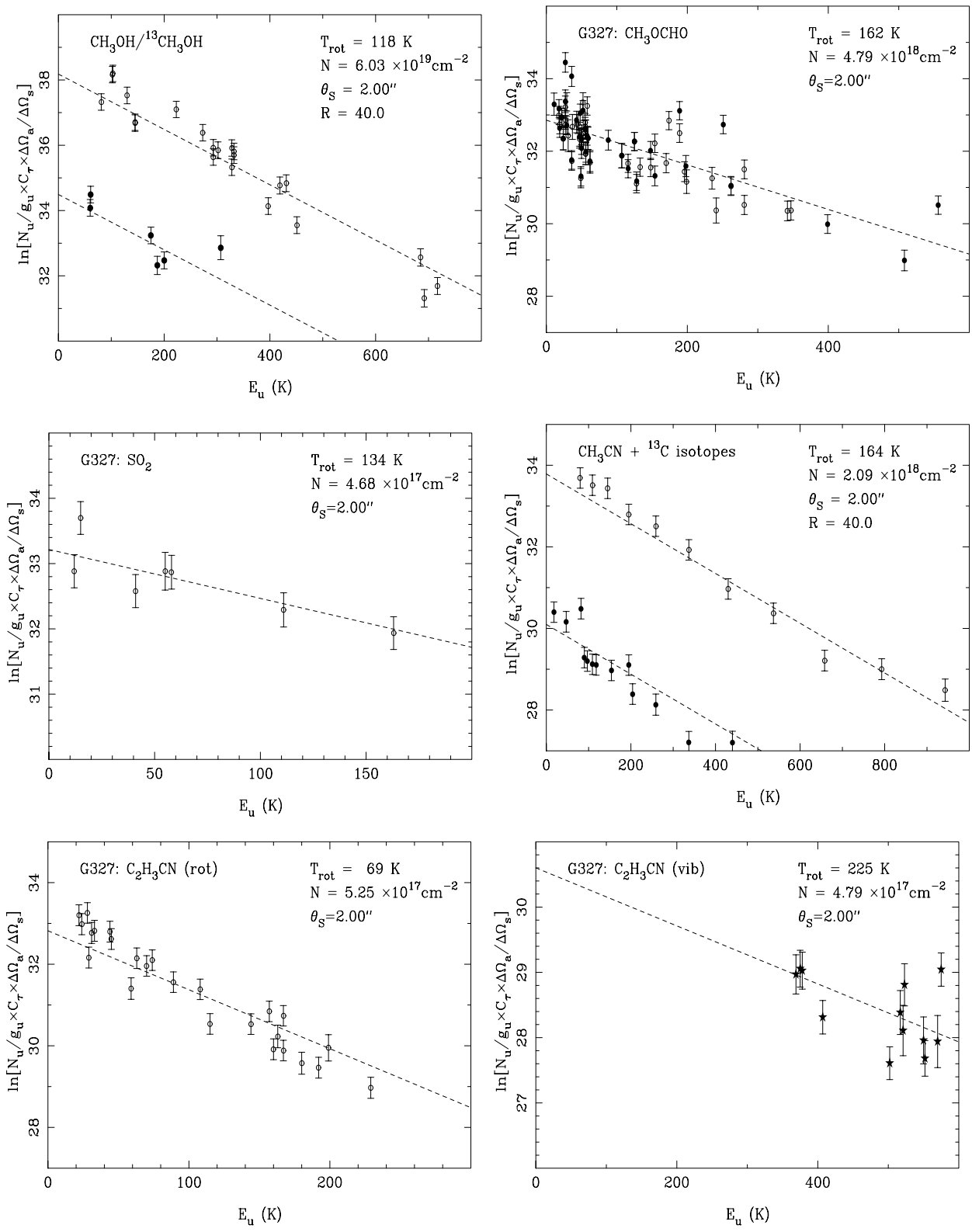

FIG. 4.—Population diagrams for molecules for which a small source size gives the best fit or for which a high-temperature component is evident. *R* is the adopted isotopic ratio discussed in § 6.1. Vinyl cyanide rotational (grnd) and vibrationally excited (vib) transitions were analyzed separately as discussed in the text (see § 6.1.1).

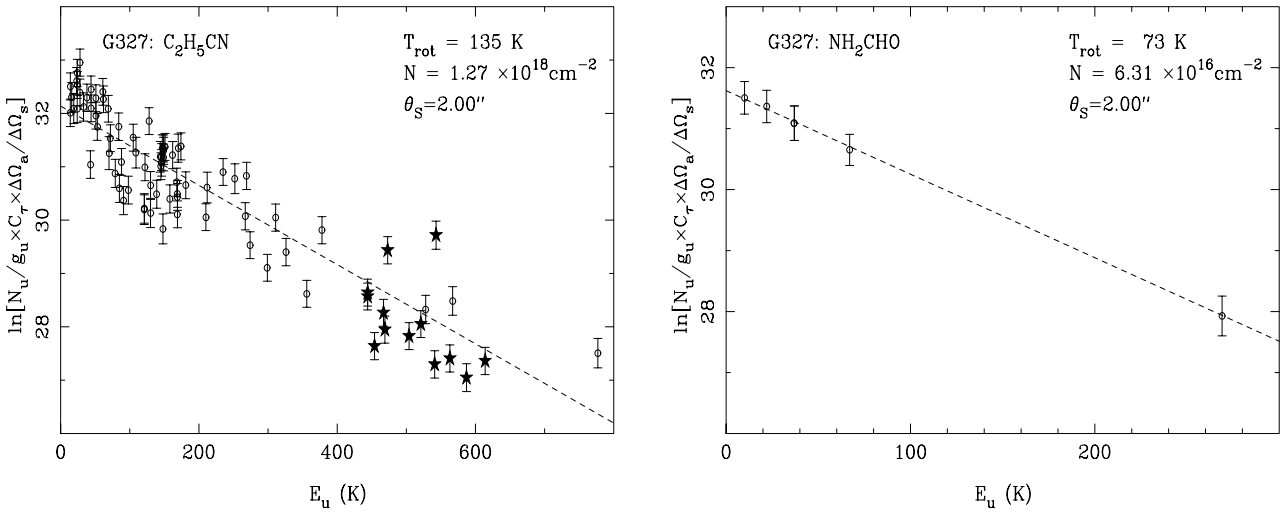

FIG. 4.—*Continued*

the homogeneous LVG best-fit models for the $6 \rightarrow 5$ and $13 \rightarrow 12$ transitions of CH_3CN and $6 \rightarrow 5$ transitions of $CH_3^{13}CN$ and $^{13}CH_3CN$ (Bergman 1992). Better results are obtained by fitting all isotopomers simultaneously, assuming $[^{12}C]/[^{13}C] = 40$. The results are shown in Tables 3 and Figure 4.

We detected 37 lines of C_2H_3CN, including 12 transitions in the first excited CCN bending mode (Nummelin & Bergman 1999). We detected 85 lines of C_2H_5CN in G327, including 13 *a*-type *R*-branch lines in the lowest CCN bending mode and the methyl torsional mode at 297 and 303 K above the ground state, respectively (see Table 4). This is the first reported detection of vibrationally excited ethyl cyanide (transition frequencies from 223.68 to 240.72 GHz). We find similar rotation temperatures to that obtained for CH_3CN (see Table 3) for both these species. Abundances for each of these species are a few times 10^{-7} in the small hot-core region (see Table 3).

TABLE 4

IDENTIFIED LINES OF METHYL MERCAPTAN AND VIBRATIONALLY EXCITED ETHYL CYANIDE

Frequency (MHz)	Transition	A_{ul} (s^{-1})	E_u/k (K)
	Methyl Mercaptan		
101284.36.....	$4_1 \rightarrow 3_1$ *E*	8.69(−6)	20
151303.27.....	$6_{-1} \rightarrow 5_{-1}$ *E*	3.12(−5)	32
151660.04.....	$6_0 \rightarrow 5_0$ *A*	3.23(−5)	25
151654.22.....	$6_0 \rightarrow 5_0$ *E*	3.23(−5)	29
151720.70.....	$6_4 \rightarrow 5_4$ *A*	1.80(−5)	95
151723.14.....	$6_2 \rightarrow 5_2$ *A*	2.88(−5)	45
151737.91.....	$6_3 \rightarrow 5_3$ *A*	2.43(−5)	66
151759.76.....	$6_{-2} \rightarrow 5_{-2}$ *E*	2.88(−5)	45
151794.86.....	$6_2 \rightarrow 5_2$ *A*	2.88(−5)	45
226286.87.....	$9_2 \rightarrow 8_2$ *E*	1.09(−4)	61
250148.09.....	$10_1 \rightarrow 9_1$ *A*	1.48(−4)	71
	Vibrationally Excited Ethyl Cyanide		
223680.4	$26_{1,25/26} \rightarrow 25_{1,24/25}$	6.80(−4)	444
223810.0	$26_{0,26} \rightarrow 25_{0,25}$	6.81(−4)	444
223964.5	$25_{8,17/18} \rightarrow 24_{8,16/17}$	5.39(−4)	521
223975.5	$25_{7,18/19} \rightarrow 24_{7,17/18}$	5.65(−4)	504
224008.9	$25_{9,16/17} \rightarrow 24_{9,15/16}$	5.07(−4)	541
224049.9	$25_{10,15/16} \rightarrow 24_{10,14/15}$	4.72(−4)	563
224093.9	$25_{11,14/15} \rightarrow 24_{11,13/14}$	4.36(−4)	587
224142.9	$25_{12,13/14} \rightarrow 24_{12,12/13}$	3.99(−4)	614
225448.3	$39_{3,36/37} \rightarrow 39_{2,38}$	1.60(−5)	543
225715.3	$25_{4,21} \rightarrow 24_{4,20}$	6.71(−4)	454
239171.0	$28_{1,28} \rightarrow 27_{2,26}$	5.58(−5)	473
240443.7	$27_{3,25} \rightarrow 26_{3,24}$	8.05(−4)	469
240718.2	$28_{0,28} \rightarrow 27_{0,27}$	8.18(−4)	467

NOTE.—$a(b) = a \times 10^b$.

4.1.2. *Sulfuretted Molecules*

Sulfuretted molecules identified in G327 include sulfur monoxide (SO, ^{34}SO), carbon monosulfide ($C^{34}S$), nitrogen monosulfide (NS), dicarbon monosulfide (CCS), carbonyl sulfide (OCS, $O^{13}CS$, $OC^{34}S$), sulfur dioxide (SO_2), thioformaldehyde (H_2CS), and the first detection of methyl mercaptan (CH_3SH) outside the Galactic center (see Table 4 for transitions). While most of these molecules have only one or two transitions for which lower limits on relative abundances were calculated (see Table 1), population diagram analysis was performed for $O^{13}CS$, $OC^{34}S$, SO_2, H_2CS, and CH_3SH. Rotation temperatures for extended emission of 53–68 K were derived for H_2CS and CH_3SH, indicating a cold-gas origin for these molecules. SO_2 and the $O^{13}CS$/$OC^{34}S$ combination, which was calculated by assuming $[^{12}C]/[^{13}C] = 40$ and $[^{32}S]/[^{34}S] = 22.5$ (Wilson & Rood 1994), resulted in temperatures greater than 100 K, indicating a hot-core origin. For SO_2 we find a small source size ($\sim 2''$), indicating that the emission is primarily from a small, hot core, as is seen for the Orion KL region (Schilke et al. 1997).

4.1.3. *Other Organic Molecules*

G327 exhibits a rich array of aldehydes, alcohols, amines, and related organic species. We have detected the formyl cation ($H^{13}CO^+$), formaldehyde (H_2CO), formic acid (HCOOH), methanol (CH_3OH, $^{13}CH_3OH$), ethanol (C_2H_5OH), methyl acetylene (CH_3CCH), methyl formate (CH_3OCHO), acetaldehyde (CH_3CHO), dimethyl ether (CH_3OCH_3), methylenimine (CH_2NH), and formamide (NH_2CHO).

HCOOH, C_2H_5OH, CH_3CHO, and CH_3CCH are best fitted as cold, extended component molecules, with rotation temperatures between 45 and 72 K. The six HCOOH lines are weak, resulting in a scattered fit. The C_2H_5OH fit is poor because of the scattered data points but gives $T_{rot} = 66$

K when assuming a filled beam. The diagrams for CH_3CHO and CH_3CCH both have little scatter. Although HCOOH, CH_3CHO, and CH_3CCH have all been detected in cold, dark clouds (Irvine, Ohishi, & Kaifu 1991), C_2H_5OH has not. Ethanol is, in fact, usually considered to be a hot-core species. This is discussed further below.

We detected 25 lines of CH_3OH and 20 lines of $^{13}CH_3OH$. Population diagram analysis of the two methanol isotopes and both *A* and *E* species together, assuming $[^{12}C]/[^{13}C] = 40$, gives $T_{rot} = 102$ K for a source size of 2.″38, evidence of a hot-core component, which is further supported by the detection of transitions with a wide range of energies above the ground state (19–692 K). For both CH_3OH and $^{13}CH_3OH$ we also analyzed the *A* and *E* transitions separately and found scattered population diagrams with rotation temperatures differing by a factor of 2. Methanol is known to maser in many transitions toward star-forming regions (Cragg et al. 1992; Sobolev, Craig, & Godfrey 1997). While some transitions that are known to maser in other sources are in our data set (e.g., $5_{-1} \rightarrow 4_0$ *E* at 84.5 GHz), they show no signs of strong masering here and cannot explain the scatter. For our analysis, we concentrated on transitions with energies greater than 50 K. The low-energy transitions have a steeper slope, suggesting that methanol has a hot-core component with a cool envelope, but the scatter prevents a satisfactory fit to a two-component model.

We identified 83 lines of methyl formate (CH_3OCHO) with energies above the ground state ranging from 8 to 556 K. If we assume a filled beam, we derive a temperature of 375 K, which is inconsistent with the large source size, which should reflect the cold-gas component. The best fit is for a smaller source size of 1.″91 and gives 170 K. Separate analysis of *A* and *E* transitions are the same to within 1 σ limits. However, the population diagram is scattered, much like that of methanol. One possible explanation for this is that different lines of CH_3OCHO originate under different physical environments. This is supported by the high range of energies above the ground state, which are not likely to originate in any single region. The high excitation transitions and high temperatures derived indicate that a component of methyl formate is present in the hot core.

We detect 19 transitions of CH_3OCH_3. The best fit is for a source size of 6.″29 and results in $T_{rot} = 50$ K. The beam-filled diagram exhibits the same high level of scatter as is evident in both methanol and methyl formate. The 2″ fit is also scattered and gives a very high 392 K rotation temperature. We note that Nummelin et al. (2000) and Turner (1991), in their analyses of Sgr B2 and Orion KL, also found these complex organic molecules to have very scattered population diagrams.

We detect five transitions of formamide, which give a best-fit rotation temperature of 72 K and a 2.″01 source size. The beam-filled diagram is a poor fit compared with the small source size.

For $H^{13}CO^+$, H_2CO, and CH_2NH, lower limits on the column density are given in Table 1.

4.1.4. *Other Species*

We also have single or double detections of carbon monoxide ($C^{17}O$), deuterated water (HDO), silicon dicarbide (*c*-SiCC), silicon monoxide (SiO), and diazenylium (NNH^+). Abundance lower limits are in Table 1.

4.2. *Relative Abundances*

Abundance lower limits for molecules with one or two transitions are shown in Table 1. Caution must be used when interpreting results based on one or two transitions. While identities of abundant molecules such as CO are unambiguous, less abundant molecules with large partition functions could be misidentified.

In order to compare abundances of molecules, a reliable H_2 column density must be determined. Abundances relative to H_2 for the extended, cooler component species were found by using $N(H_2) = 3.2 \times 10^{23}$ cm^{-2} as derived by Bergman (1992) using equation (1) with observations of the $J = 1 \rightarrow 0$ transitions of $^{12}C^{18}O$ and $^{13}C^{18}O$ and assuming a 50 K temperature and $X[^{12}C^{18}O] = 2 \times 10^{-7}$ and $X[^{13}C^{18}O] = X[^{12}C^{18}O]/40$. This value may be an underestimate since the $^{12}C^{18}O$ line may be somewhat optically thick.

As an independent check, we used the value of $T_{eff} \sim$ 36,000–40,000 K estimated by Ehrenfreund et al. (1997) from *ISO* observations, which implies a central star with spectral type in the range O6–O8. We therefore assumed a single star of spectral type O7 and absolute magnitude $M_V = -5.2$ (Schmidt-Kaler 1982). We use the standard magnitude-distance equation

$$m - M - A = 5 \log d - 5 \quad (10)$$

to evaluate extinction *A* independently in each of two passbands (*H*: 1.65 μm and *K*: 2.2 μm), using photometry from the Catalog of Infrared Observations (Gezari, Schmitz, & Mead 1987) and assuming the kinematic distance $d \approx 2900$ pc to G327 (Simpson & Rubin 1990). Intrinsic $V-H$ and $V-K$ colors appropriate to an O7 star were taken from Wegner (1994). The standard mean extinction law was then used to evaluate visual extinction A_V, and total (atomic + molecular) hydrogen column density was then estimated from the mean correlation for the local interstellar medium, $N(H)/A_V \approx 1.9 \times 10^{21}$ cm^{-2} mag^{-1}, e.g., Whittet (1992). The *H* and *K* passbands gave consistent results, yielding average values of $A_V \sim 36$ mag and $N(H) \sim 7 \times 10^{22}$ cm^{-2}. These are lower limits, as there may be more than one star illuminating the H II region: for example, if four identical O7 stars are assumed, $A_V \sim 50$ mag and $N(H) \sim 1 \times 10^{23}$ cm^{-2}. These results are therefore consistent with the value of $N(H_2) \sim 3 \times 10^{23}$ cm^{-2} discussed above.

The hot-core species listed in Table 3 were all found to have an effective source size between 1.″42 and 2.″38. Since no direct comparison of column densities or abundances is meaningful between species with different source sizes, we set the source size equal to the average size of 2″ in our analysis. In order to estimate the H_2 column density for the ultracompact core, we used the model by Bergman (1992) (Fig. 1), who estimated $n(H_2)$ to be in the range 2×10^7–10^8 cm^{-3} in the hot-core region, 2×10^6–10^7 cm^{-3} in the outer hot core, and 10^6 cm^{-3} in the envelope. Using the average of these values, we integrated through the central 2″ (8.7×10^{16} cm). The resulting column density is $\sim 3 \times 10^{24}$ cm^{-2}. This 10-fold increase in H_2 column density over a decrease in source size from 20″ to 2″ is consistent with that found in Sgr B2 (Nummelin et al. 2000). When making abundance comparisons, one must keep in mind that this value is uncertain. The hot-core H_2 column density can

range from 1 to 6 ($\times 10^{24}$) cm^{-2}, making our abundances uncertain by at least a factor of 2.

5. THE DISTRIBUTION OF MOLECULES IN G327

As was found by Bergman (1992), the emission from the $C^{18}O$ ($J = 2 \rightarrow 1$ and $1 \rightarrow 0$) transitions extends over more than $4' \times 5'$ around the hot-core position. In contrast, Bergman found the CH_3CN emission to be much more compact and significantly peaked at the hot core. To put further constraints on the chemistry in the hot core of G327, we mapped two bands of ethyl cyanide, containing lines in the $J = 12 \rightarrow 11$ and $J = 26 \rightarrow 25$ rotational ladders, respectively. The latter band contains 18 detected C_2H_5CN lines, as well as a number of lines from other species. In Figure 5 gray-scale/contour maps of the integrated line intensities of four of the detected lines are shown. These four lines have energies above the ground state of 33, 205, 471, and 574 K (in the first torsionally excited state) and should thus sample progressively warmer gas. Fitting of a two-dimensional Gaussian to the emission in each map yields sizes (FWHM) in the range $35'' \times 28''$–$52'' \times 46''$, where the lower value was obtained for the $26_{10,16/17} \rightarrow 25_{9,15/16}$ $v_t = 1$ line and the higher one for the $12_{0,12} \rightarrow 11_{0,11}$ line. This indicates unresolved or marginally resolved, slightly north-south or northeast-southwest elongated emission in all of these lines by the 22″ or 48″ antenna main beam. Considering the lower angular resolution, 48″, in the $12_{0,12} \rightarrow 11_{0,11}$ map (at 105 GHz), the small-scale structure should not be considered significant. The peak of the emission corresponds to the hot-core position in all maps except that for the torsionally excited line, which peaks approximately 10″ southwest of the (0, 0) position. Because of the generally very high H_2 densities required for collisional excitation of vibrational states, these states are often considered to be excited by far-infrared radiation. The first torsionally excited state of C_2H_5CN is excited by radiation from around 48 μm. Hence, the rotational lines within the torsionally excited state could be tracing the radiation field, which is one possible explanation for the slight difference in the distribution of emission as compared with the ground-state lines.

Similar marginally resolved source sizes were also found for lines of CH_3OCHO and CH_3OH, which were serendip-

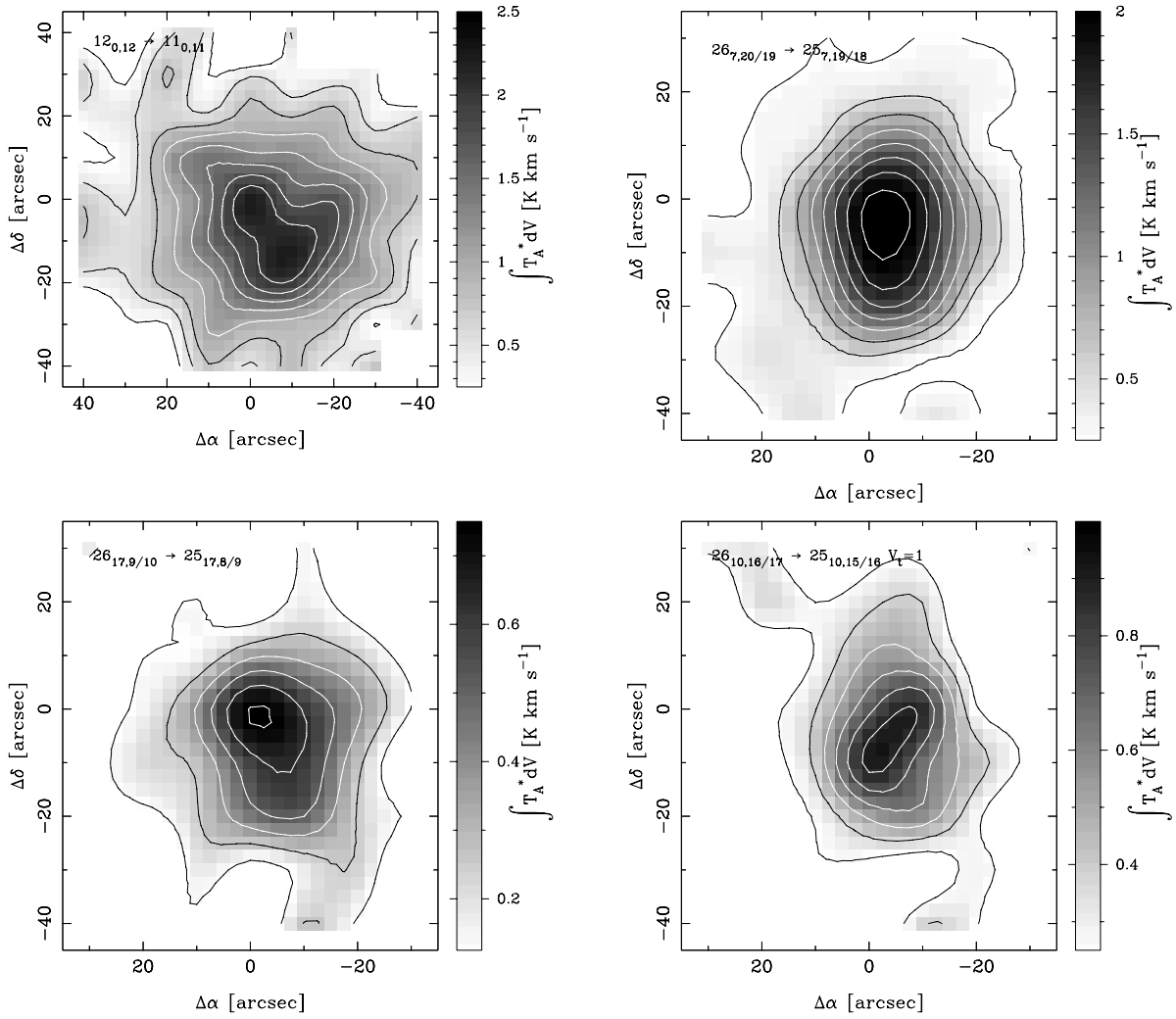

FIG. 5.—Maps of the C_2H_5CN emission in G327, centered on the hot-core position [$\alpha(1950) = 15^h49^m15^s.6$, $\delta(1950) = -54°28'07''$]. The lowest contours and contour increments are (*upper left and upper right*) 0.25 and 0.25 K km s^{-1}, (*lower left*) 0.125 and 0.125 K km s^{-1}, and (*lower right*) 0.25 and 0.125 K km s^{-1}. Intensity is given in the T_A^* scale. The four lines shown have upper-state energies of 33, 205, 471, and 574 K, respectively. The 33 K line, at a rest frequency of 105.47 GHz, has a lower angular resolution, 48″, as compared with the higher energy lines around 233.2 GHz, which have 22″ resolution.

itously located within the mapped $J = 26 \rightarrow 25$ ethyl cyanide band. The relatively small source sizes found for all of these species are consistent with a possible dust origin. However, it is clear that arcsecond or subarcsecond resolution would be necessary for a more detailed study of the small-scale structure of the hot core in G327.

6. DISCUSSION

G327 is a source very rich in complex saturated molecules. It is interesting to note that many of the molecules show transitions from levels with energies greater than 100 K above ground, even up to ~900 K for a transition of CH_3CN, clearly indicating the presence of a region of very hot gas and dust. Most molecules fall into one of three categories. There are those hot-core molecules that have many excited high-energy transitions and for which a high rotation temperature and small effective source size are derived. These molecules include the nitriles (CH_3CN, C_2H_3CN, C_2H_5CN) and NH_2CHO. Rotational temperatures and column densities for these molecules are listed in Table 3 with comparisons to Sgr B2 and OMC-1 column densities in Table 5. The second category includes C_2H_5OH, CH_3OCH_3, and CH_3OCHO, which also have high-energy transitions indicative of a hot component, but the transitions are too scattered to fit a convincing population diagram to a small source. Methanol also has a wide range of transitions, but when we use only transitions with excitation energies above 50 K we find a compact source and one of the highest abundances reported to date. These molecules are consistent with enhanced hot-core abundances surrounded by a cooler envelope of emission. There are also molecules for which the best fit is for extended emission (over our full beam) and a low temperature. These molecules include OCS, H_2CS, CH_3CCH, and HCOOH. Table 6 compares abundances of these molecules in G327 with the sources G34.3+0.15, G5.89−0.39, Sgr B2, OMC-1, and W3 (H_2O).

6.1. *Chemistry*

6.1.1. *Nitriles*

HC_3N is thought of as a cold-cloud tracer but should also be formed efficiently in the hot gas if C_2H_2 is evaporated from grain mantles (Millar et al. 1997). According to current chemical models, HC_3N is produced in the hot gas by reaction of C_2H_2 with CN or N with C_3H_2 (Millar, Macdonald, & Gibb 1997; Tielens & Charnley 1997). CH_3CN is a symmetric top molecule likely formed via radiative association of CH_3^+ with HCN or CN with CH_3 (Charnley et al. 1992; Millar et al. 1997). It should be efficiently frozen onto icy grain mantles at the low temperatures of 40 K or less found in dark interstellar clouds. It could also be formed in the mantle by hydrogenation of accreted CCN (Caselli et al. 1993). Our beam-averaged CH_3CN abundance is very well determined, as may be seen from the simultaneous fitting of both main and ^{13}C isotopes in Figure 4. Nonetheless, the beam-averaged methyl cyanide abundance in G327 is 2 orders of magnitude greater than in G34, 6 times greater than in the Orion compact ridge, and 7 times higher than in the Orion hot core. The physical size for the G327 observations is larger than these sources (0.32 pc compared with 0.21 and 0.034 pc, respectively), indicating an even greater abundance discrepancy due to beam dilution. Nummelin et al. (2000), in their Sgr B2 study, determined CH_3CN abundances for source sizes equivalent to ~0.08 and 0.05 pc for the N and M hot cores, respectively (see Table 5). G327 abundances for a slightly smaller region (~0.03 pc) are 1 order of magnitude higher. Hence, G327 is a particularly rich source of the nitrile CH_3CN, at least as rich in this regard as the well-studied Sgr B2.

Nitrile molecules such as C_2H_3CN and C_2H_5CN have

TABLE 5

ABUNDANCE COMPARISONS OF HOT-CORE MOLECULES

		Sgr B2 (N)[b]		Sgr B2 (M)[b]		OMC-1[c]	
SPECIES	G327.3−0.6[a] Abundance	Abundance	Size (pc)	Abundance	Size (pc)	Compact Ridge Abundance	Hot Core Abundance
NS	>7(−10)	1(−8)	0.098	...	...	...	...
SO	>4(−10)	2(−8)	0.13	1(−7)	0.17	3(−7)	2(−7)
^{34}SO	>1(−11)	1(−9)	0.13	4(−9)	0.17	...	...
SO_2	1(−7)	3(−8)	0.079	4(−7)	0.088	2(−7)	1(−7)
$^{34}SO_2$	...	4(−9)	0.079	2(−8)	0.088	...	...
H_2CS	...	2(−8)	0.082	...	...	1(−9)	8(−10)
CH_3OH	2(−5)	2(−7)	0.062	2(−7)	0.031	4(−7)	1(−7)
CH_2NH	>3(−11)	1(−8)	0.082	...	...	9(−11)	7(−11)
HC_3N.....	>8(−11)	5(−9)	0.11	3(−9)	0.079	6(−9)	2(−9)
$HC^{13}CCN$.....	>6(−12)	6(−10)	0.11	4(−10)	0.079	...	...
$HCC^{13}CN$.....	>1(−11)	1(−9)	0.11	3(−10)	0.079	...	...
CH_3CN.....	7(−7)	3(−8)	0.082	2(−8)	0.049	5(−9)	4(−9)
$^{13}CH_3CN$	4(−8)	3(−9)	0.082	1(−9)	0.049	...	...
$CH_3^{13}CN$	1(−8)	5(−9)	0.082	...	...	...	...
C_2H_3CN.....	2(−7)[e]	6(−8)	0.022	...	...	1(−9)	2(−9)
C_2H_5CN.....	4(−7)	1(−8)[d]	0.028	...	...	5(−9)	...

NOTE.—$a(b) = a \times 10^b$.

[a] Using 2″ (0.028 pc) source size abundances. Lower limits are calculated from Table 1 using $N(H_2) = 3 \times 10^{24}$ cm^{-2}.

[b] Values from Nummelin et al. 2000.

[c] From Sutton et al. 1995. Values correspond to a 0.034 pc source size.

[d] From Liu & Snyder 1999.

[e] Abundances are the same for both rotational and vibrational lines treated separately with a 2″ source size.

TABLE 6

ABUNDANCE COMPARISONS IN SEVERAL SOURCES

				Sgr B2[d]			OMC-1[e]		
SPECIES	G327.3−0.6[a]	G34.3+0.15[b]	G5.89−0.39[c]	N	M	NW	Compact Ridge	Hot Core	W3(H$_2$O)[f]
C^{17}O	>7(−8)	>2(−8)	...	2(−8)	4(−8)	2(−8)	...	...	...
H^{13}CO$^+$	>2(−11)	>2(−11)	>6(−9)	4(−12)	3(−11)	2(−11)	...	...	...
HCOOH	3(−10)	>2(−9)	...	1(−10)	...	...	1(−9)	8(−10)	...
CH$_3$OH	7(−8)	7(−8)	1(−6)	3(−9)	6(−9)	1(−8)	4(−7)	1(−7)	5(−8)
^{13}CH$_3$OH	5(−9)	1(−9)	...	3(−10)	3(−10)	...	...	...	...
CH$_3$CHO	5(−10)	...	...	2(−10)[i]	2(−10)[i]	...	<2(−10)[g]	...	...
C$_2$H$_5$OH	3(−9)	7(−9)	...	1(−9)	6(−10)	2(−9)	2(−9)	7(−10)	...
CH$_3$OCHO	5(−8)	3(−8)	...	1(−9)[i]	9(−10)[i]	...	3(−8)	1(−8)	3.5(−9)
CH$_3$OCH$_3$	3(−8)	...	...	3(−9)	2(−9)	...	2(−8)	8(−9)	1(−8)
CH$_3$CCH	7(−9)	3(−8)	2(−7)	4(−9)	5(−9)	2(−9)	1(−9)	1(−9)	3(−9)
CH$_2$NH	>3(−10)	>8(−10)	...	...	2(−10)	1(−10)	9(−11)	7(−11)	...
NH$_2$CHO	3(−10)	...	...	2(−10)[i]	1(−10)[i]	...	3(−10)	1(−10)	...
H^{13}CN	>3(−10)	>3(−11)	...	...	...	2(−11)	...	...	...
HNCO	>2(−10)	>5(−10)	...	6(−10)	1(−9)	3(−9)	...	6(−9)[g]	3(−9)
HC$_3$N	>2(−10)	>5(−11)	2(−7)	...	4(−10)[h]	2(−9)	6(−9)	2(−9)	8(−11)
HC^{13}CCN	>6(−11)	...	...	...	...	...	...	...	...
HCC^{13}CN	>1(−10)	...	...	...	...	...	...	...	...
CH$_3$CN	3(−8)	5(−10)	4(−7)	...	...	4(−11)	5(−9)	4(−9)	1(−10)
C$_2$H$_3$CN	2(−9)	8(−9)	...	4(−10)	...	...	1(−9)	2(−9)	...
C$_2$H$_5$CN	8(−9)	>9(−10)	...	6(−10)[i]	1(−10)[i]	...	5(−9)	1(−8)[g]	...
C^{34}S	>2(−10)	>1(−10)	>4(−8)	6(−11)	1(−10)	7(−11)	...	...	...
NS	>7(−9)	>8(−11)	...	...	3(−10)	1(−10)	...	...	...
SO	>3(−9)	2(−9)	>1(−6)	...	1(−8)[h]	1(−9)	3(−7)	2(−7)	7(−9)
^{34}SO	>1(−10)	>2(−10)	>1(−7)	...	...	...	...	...	...
SO$_2$	2(−10)	3(−9)	1(−6)	...	2(−8)[h]	4(−10)	2(−7)	1(−7)	5(−9)
^{34}SO$_2$	...	2(−9)	3(−7)	...	...	...	...	...	...
OCS	>2(−9)	>3(−9)	>1(−7)	2(−9)	3(−9)	2(−8)	3(−8)	1(−8)	...
OC^{34}S	1(−9)	>8(−10)	...	3(−10)	3(−10)	...	...	...	...
O^{13}CS	7(−10)	>9(−10)	...	7(−10)	6(−10)	...	...	...	...
H$_2$CS	1(−9)	2(−9)	>5(−7)	...	4(−10)	3(−10)	1(−9)	8(−10)	8(−10)
CH$_3$SH	7(−10)	...	...	4(−10)	5(−10)	...	...	...	...
HDO	>4(−12)	>4(−9)	...	4(−10)	4(−10)	...	4(−8)	1(−8)	...
SiO	3(−11)	...	...	2(−11)	6(−11)	3(−11)	8(−9)	6(−9)	3(−10)

NOTE.—$a(b) = a \times 10^b$.

[a] Using beam-averaged abundances, corresponding to a source of 0.32 pc.

[b] Using values from Macdonald et al. 1996 for a 0.21 pc source.

[c] Values from Thompson & Macdonald 1999 for a 0.25 pc source. Note: these values are based on the $n(H_2) = 10^4$ cm^{-3} of Gomez et al. (1991), which was derived by assuming $[NH_3]/[H_2] = 10^{-5}$. However, G5.89 has one of the lowest NH_3 abundances seen in ultracompact H II regions (Cesaroni, Walmsley, & Churchwell 1992), probably giving abundances which are 10–100 times too high.

[d] Values from Nummelin et al. 2000 for a 0.79 pc source.

[e] Values from Sutton et al. 1995 for a 0.034 pc source.

[f] Values from Helmich & van Dishoeck 1997 for a 0.23 pc source.

[g] Values from Blake et al. 1987 for a 0.073 pc source. Note: these values are smaller than Sutton et al. 1995 values since they include only a narrowly defined kinematic component while Sutton et al. 1995 includes quiescent values along the line of sight.

[h] Values from Kuan & Snyder 1996.

[i] Using *a*-type transitions only.

high abundances in many hot cores that cannot be reproduced by gas phase reactions alone. C_2H_3CN is also detected via its rotational lines in both giant molecular and dark clouds. Such reactions as

$$HC_3NH^+ + H_2 \rightarrow C_2H_3CN^+ + H\,, \qquad (11)$$

$$C_2H_3CN^+ + H_2 \rightarrow C_2H_4CN^+ + H, \quad \text{etc.}\,, \qquad (12)$$

are endothermic and proceed slowly in the gas phase (Blake et al. 1987), though C_2H_3CN may be formed by reactions of CN and evaporated C_2H_4 in the hot gas (Charnley et al. 1992). Charnley et al. (1992) concluded in their analysis of the hot cores in Orion A that C_2H_5CN abundances could not be reproduced by gas-phase chemistry and hypothesized that the hydrogenation of accreted HC_3N and CH_3CN would produce C_2H_5CN, which would evaporate when heated. This method of production may be so efficient that Caselli et al. (1993), in their model of the Orion hot core, predict that C_2H_5CN becomes the most abundant mantle constituent at the end of core collapse. Liu & Snyder (1999) studied C_2H_3CN and C_2H_5CN in the hot core Sgr B2(N) at 85 GHz using the Berkeley-Illinois-Maryland Association Array at 0.″8 resolution, corresponding to physical scales 1/10 the size of the Oort cloud. They concluded that their high column densities for these molecules, 3 times higher than previously reported, were indicative of a high core concentration of these species, providing further support for an icy origin. Liu & Snyder (1999) estimate an abundance of $\sim 10^{-8}$ for both C_2H_3CN and C_2H_5CN for a $\sim$6000 AU ($\sim$0.03 pc) source size. The same physical size for G327 corresponds to a $\sim 2''$ source size. Nummelin et al.

(2000) report an abundance for C_2H_3CN of 6×10^{-8} for an estimated 0.022 pc source size. The corresponding fractional abundances we estimate are 2×10^{-7} and 4×10^{-7} cm^{-2} for C_2H_3CN and C_2H_5CN, respectively (see Table 5). This would seem to indicate that these hot-core nitrile molecules truly are close to 1 order of magnitude more abundant in G327 than in Sgr B2, consistent with our results given above for CH_3CN.

It was noted by Liu & Snyder (1999) that C_2H_3CN was observed preferentially in the outflow of Sgr B2, and they suggest that C_2H_5CN is processed into C_2H_3CN in shock regions. The vibrationally excited vinyl cyanide transitions could be due to collisions or infrared radiation from hot dust. The different physical processes, coupled with the distinctly separate temperature regimes covered by rotational and vibrational lines, suggest that the different transitions should be treated separately. Indeed, when both are analyzed together, the results are inconsistent, giving low temperatures and unphysically high abundances. In Figure 4 we show 2″ population diagrams for the rotational and vibrational transitions separately. The rotational transitions give a good fit with a relatively cool $T_{\rm rot}$ of 69 K and a column density of 5.3×10^{17} cm^{-2}. The vibrational transitions result in a much warmer (225 K) temperature but a similar column density (4.8×10^{17} cm^{-2}).

The CH_3CN maps made by Bergman (1992) and the C_2H_5CN maps shown in § 5 clearly show that the abundances of CH_3CN and C_2H_5CN are much greater in the hot core than in the surrounding region of cooler gas as traced by CH_3CCH. This is also consistent with grain surface reactions and evaporation of grain surface products being responsible for the overabundance.

It is interesting, in light of all the gas-phase inferences to solid nitriles, to note that there is little evidence in infrared data for solid nitrogen-bearing molecules. N_2 is thought to be present but is infrared inactive and hence very difficult to detect. There are also two indications, in massive protostars W33 A and NGC 7538 IRS9, of NH_3 (Lacy et al. 1998; Gibb et al. 2000). A feature present at 4.62 μm in several embedded protostars has yet to be unambiguously identified and is designated as "XCN." A possible candidate is the OCN^- ion (Schutte & Greenberg 1997; Pendleton et al. 1999). Laboratory studies have shown that this feature can be produced only by UV photolysis or ion irradiation of ice mixtures containing both N and C, and it is attributed to the C≡N stretch mode (see Pendleton et al. 1999 for a recent review). Bernstein et al. (1995) also report a probable vinyl cyanide feature formed by photolysis of ice mixtures containing H_2O, CO, NH_3, and CH_3OH, which sublimates when the ices are warmed. Laboratory spectra of frozen nitriles show that the C≡N stretch should have a peak position between 4.35 and 4.55 μm, while isonitriles peak between 4.59 and 4.67 μm (Bernstein, Sandford, & Allamandola 1997). It would appear that the nitriles observed in the gas phase cannot account for the XCN feature, and thus far *ISO* observations have not detected nitrile features in the 4.35–4.55 μm range where these molecules would be expected to have infrared absorption features.

This leads to an interesting question that needs to be addressed. If the abundant nitriles in the gas phase must be explained by an icy origin, then why are they not seen in ice spectra of protostellar regions? If we assume, as an example, that all the gas-phase CH_3CN in G327 came from the polar constituent of the grain mantle, then we would expect to see features at 2296 and 2264 cm^{-1} (4.36 and 4.42 μm) with FWHM of 15 cm^{-1} (0.03 μm) in similar sources that have not yet undergone grain evaporation. The integrated absorbance in a water matrix for CH_3CN is 1.1×10^{-17} cm molecule^{-1} (Bernstein et al. 1997). Using the equation

$$N = \frac{\int \tau_i(v)dv}{A_i}, \tag{13}$$

where τ_i is the optical depth and A_i is the integrated absorbance, and taking the column density of methyl cyanide for the best-fit source size of 1.″42 (Table 3) results in an ice feature with an optical depth of $\sim$1.3 prior to evaporation. A similar calculation for C_2H_3CN ($A_i = 7.7 \times 10^{-18}$ cm molecule^{-1}) gives a feature at 4.46 μm with an FWHM of 16 cm^{-1} and an optical depth of 0.2 and 2.1 for the abundances deduced from ground-state rotational and vibrationally excited transitions, respectively. Band strengths are not available for C_2H_5CN, but if we assume an average nitrile band strength of 10^{-17} and an FWHM of $\sim$15 cm^{-1}, then a similar feature of optical depth $\sim$1 would be expected. All these nitriles together, if abundant enough, would result in a broad feature in the 4.3–4.6 μm spectrum. If similar column densities of nitriles were present in a less evolved source in which the ices have not evaporated, these features should certainly be detectable by *ISO*. No young stellar objects studied to date show features at these wavelengths.

Laboratory data point to the necessity of a matrix containing C- and N-bearing molecules such as methanol and ammonia as well as a UV radiation field in order to produce various CN-bearing molecules. The temperature for complete grain evaporation of N-bearing molecules such as C_2H_3CN and C_2H_5CN is about 50 K (Caselli et al. 1993). After accretion in the cold collapse phase, the temperature increases and rapid loss of the ice mantle follows. This evaporation would occur in an expanding shell around the source as the core temperature increases, heating the surrounding material. This short lifetime on the grain surface could explain why nitriles are not seen in abundance in the infrared.

Above we discussed the high abundance of CH_3CN, C_2H_3CN, and C_2H_5CN in G327 compared with other sources. It could be that G327 and Sgr B2, another nitrile-rich source, are atypical in their high abundances and that most protostellar sources have lower nitrile abundances. This might contribute to the lack of detections in infrared observations.

6.1.2. *Sulfuretted Molecules*

H_2CS is formed via such gas phase reactions as (Charnley 1997)

$$S + CH_3 \rightarrow H_2CS + H \tag{14}$$

and

$$H_3CS^+ + e^- \rightarrow H_2CS + H\,. \tag{15}$$

In the model by Taylor, Morata, & Williams (1998), H_2CS is characterized as an early-time molecule, one that peaks in abundance prior to 2×10^6 yr into collapse. These predicted high peak abundances have not yet been observed, and the chemistry of this molecule could be complicated by a grain surface origin of some H_2CS. The abundance of this

molecule in G327 is comparable to that in G34 and midway between those in Sgr B2 N, M, and the OMC-1 compact ridge.

The sulfur analog of methanol, methyl mercaptan (CH_3SH), has been detected toward the hot cores in Galactic center source Sgr B2 (Linke, Frerking, & Thaddeus 1979; Nummelin et al. 2000) with an abundance similar to that of G327, but thus far only upper limits have been calculated for dark clouds and other hot cores. While the chemistry of methyl mercaptan is not understood, it may be formed on grain surfaces with a process analogous to the hydrogenation of CO that is thought to form CH_3OH (Bettens et al. 1999). As long as CH_3SH exists in grain mantles, it should be evaporated in hot cores.

SO_2 is the result of destruction of H_2S by H_3O^+, which eventually leads to the release of S atoms that can then react and combine with OH and O_2 (Charnley 1997). G327 has a lower abundance of SO_2 than any of the other sources in Table 6 but is closest to Sgr B2 (NW), which is sampling the envelope of this giant molecular cloud. The low SO_2 abundance coupled with high abundances of complex molecules support the view that G327 is in a much earlier phase of postevaporation chemistry than most other hot cores observed to date.

OCS is primarily formed in the gas phase by the radiative association reaction

$$\mathrm{CO} + \mathrm{S} \rightarrow \mathrm{OCS} + h\nu\,, \tag{16}$$

at early stages of cloud collapse ($t \leq 2 \times 10^4$ yr), after which it is formed primarily by

$$\mathrm{HOCS}^+ + e^- \rightarrow \mathrm{OCS} + \mathrm{H} \tag{17}$$

(Charnley 1997). There is a tentative detection of solid OCS on the dust grains toward massive protostellar object W33 A (Palumbo, Tielens, & Tokunaga 1995). Detections of gas-phase OCS by Nummelin et al. (1998) in Sgr B2 show that, while OCS is present in cold-cloud regions, it is sharply peaked toward the hot core. We estimate a hot-core abundance of $\sim 2 \times 10^{-8}$ for OCS, which is very similar to that found in the OMC-1 hot core and compact ridge (see Table 5).

6.1.3. *Other Organic Molecules*

It is interesting to compare abundances of oxygen-bearing organic species between G327 and other sources. Oxygen-bearing organic species including HCOOH, CH_3OH, CH_3CHO, C_2H_5OH, CH_3OCHO, and CH_3OCH_3 are more abundant in G327 than in Sgr B2 N, M, or NW, by 1 order of magnitude or more for CH_3OCHO and CH_3OCH_3. In fact, those two molecules are more abundant in G327 than in any of the other sources listed in Table 6. This high abundance of saturated molecules implies recent grain evaporation and that G327 could therefore be in a younger evolutionary state.

Chemical models have C_2H_5OH being formed by H and C addition to CO on ice mantles (Charnley et al. 1995). Millar et al. (1997) investigated C_2H_5OH formation via dissociative recombination of $C_2H_5OH_2^+$ in hot gas, which is in turn formed from reactions of H_3O^+ with evaporated C_2H_4, and found this route to be inadequate to explain observed abundances. Currently, there are no hot gas-phase chemical pathways that can reproduce ethanol abundances in hot cores. In either case, it would be expected that the ethanol abundance would be strongly peaked toward the hot core. Further observations would be needed to verify this.

Current interstellar chemistry theory has methanol being formed by hydrogenation of CO on a grain before being evaporated into the gas upon heating by a forming star (Charnley et al. 1992). Recent *ISO* observations have shown grain mantle CH_3OH abundances with respect to water ice of $\sim$30% for RAFGL 7009S and $\sim$18% for W33 A (Dartois et al. 1999; Gibb et al. 2000), both high-mass protostars. Other objects from comets to dark clouds to low-mass star formation regions have methanol abundances not exceeding 6% that of water ice (Gibb et al. 2000). This is consistent with efficient CH_3OH formation only by energetic or thermal processing in the vicinity of massive YSOs. It is expected, therefore, that the abundance of methanol will rise sharply toward the central region of a hot core where it is formed and evaporated (Ehrenfreund et al. 1998). Our high methanol abundance in the hot core is consistent with this idea, but a conclusive test requires higher angular resolution. A good observational test would be subarcsecond resolution maps made with the Atacama Large Millimeter Array (ALMA), a 64-antenna array scheduled to be built in Chile's Atacama desert sometime this decade, to determine whether there is a steep gradient in abundance near the core.

Our hot-core CH_3OH abundance is higher, in many cases by more than 1 order of magnitude, than in the other sources listed in Table 6 with the exception of G5.89. However, as is noted in the table, the reported abundances in this source are likely 10–100 times too high. If the methanol is located primarily within 2″ of the core position, the abundance is even higher (2×10^{-5}; see Table 5). This result is roughly similar to the methanol abundances as high as 7×10^{-6} found by Bachiller et al. (1995) in outflows of shocked gas. Caselli et al. (1993) calculated abundances in a model of the Orion compact ridge of 2×10^{-5} at an age of $\sim 10^5$ yr. In additon, Cernicharo et al. (1999) find a water abundance of $\sim 10^{-5}$ in Orion IRC 2 and Sgr B2, and Elias 16 results suggest that the fractional abundance of H_2O in grains $\approx 8.6 \times 10^{-5}$ (Whittet 1992). These results for water, coupled with the evidence of 10%–30% methanol abundances with respect to water on solid grain mantles in massive star-forming regions discussed above, indicate that gas-phase abundances for CH_3OH of 10^{-5} are not unreasonable.

Acetaldehyde formation can proceed by different routes in different parts of the cloud. In the model of G34 by Millar et al. (1997), neutral-neutral reaction of O atoms and C_2H_5 dominates in the ultracompact core. This is based on the assumption of evaporated C_2H_6 undergoing proton transfer reactions to form the C_2H_5 radical. In the compact core, recombination of CH_3CHOH^+ is theorized to form CH_3CHO, though the formation of this reactant has yet to be studied in a laboratory. Another possibility is that suggested by Tielens & Charnley (1997), by which H and C additions to CO ice proceed to form many hydrocarbons, including acetaldehyde.

Blake et al. (1987) theorize that CH_3OCHO is formed efficiently in hot gas by reactions with desorbed methanol. Our derived 162 K temperature and 2″ source size and the poor fit to a beam-filled source support this theory.

Dimethyl ether, CH_3OCH_3, the isomer of C_2H_5OH, is formed by reaction of CH_3OH with $CH_3OH_2^+$ (Millar et al.

1997) or by dissociative recombination of $CH_3OCH_4^+$ (Charnley et al. 1992). If we assume that CH_3OH is formed in abundance on grains and then evaporated, CH_3OCH_3 should be more abundant than C_2H_5OH since its parent molecules would be more abundant. This appears to be the case in G327. The significant enhancement of CH_3OCH_3, CH_3OCHO, and CH_3OH abundances supports the view that these molecules are chemically linked in hot cores (Blake et al. 1987; Minh et al. 1993).

Methyl acetylene, or propyne, CH_3CCH, is a symmetric top molecule. Hatchell et al. (1998), in their survey of ultracompact H II regions, claim that the high-energy CH_3CCH transitions trace hot gas and should originate in a compact region when compared with CO emission, but a larger region than CH_3CN emission. In OMC-1, CH_3CCH is not detected in the hot core or compact ridge but only in the extended ridge with an inferred rotation temperature of 52 K (Blake et al. 1987). Although we detect some transitions from levels up to 201 K above the ground state, our best fits are for extended emission.

Formamide is most likely formed by atom addition to HCO on grain mantles and then evaporated (Tielens & Charnley 1997), which is supported by the excellent fit to a source size of 2″ derived for this molecule. Bernstein et al. (1995) found NH_2CHO to be formed upon UV photolysis and warm-up of a $H_2O:CH_3OH:CO:NH_3 = 100:50:10:10$ mixture. By using ^{13}C-tagged methanol, Bernstein et al. (1995) determined that most of the carbon in the complex molecules formed during photolysis and warm-up came from methanol. While the methanol abundance in this mixture is higher than that found in any astrophysical context to date, it is closest to what has been found for high-mass protostars such as RAFGL 7009S and W33 A and supports grain formation and evaporation in massive YSO environments as a likely source for NH_2CHO.

6.2. *Conclusion*

Hot cores have a very rich chemistry with high abundances of saturated molecules. The chemical pathways discussed above (§ 6.1) predict that many molecules, including C_2H_3CN, C_2H_5CN, NH_2CHO, and CH_3OH, should be formed via atom addition to simpler molecules in the icy mantles of dust grains that are deposited during the cold collapse phase of protostar formation (Charnley et al. 1992; Caselli et al. 1993; Tielens & Charnley 1997). During collapse and formation of a luminous stellar body, the dust and gas heat up and are exposed to ultraviolet radiation, causing thermal polymerization or photolysis of new, mostly saturated species that are then released back into the gas phase (Bernstein et al. 1995; Sandford et al. 1997). Our results are consistent with this picture. We derive column densities of $\sim 10^{16}$–10^{19} cm^{-2}, higher than predicted by hot gas-phase reaction models alone, and source sizes on the order of 0.02–0.03 pc for these complex species.

We have reported the first detections of methyl mercaptan outside the Galactic center and vibrationally excited ethyl cyanide and have demonstrated that the hot core G327 is a very rich source with the highest abundance of methanol yet reported and high abundances of several nitrile species and other organics. Its relatively simple physical structure gives narrow, Gaussian line profiles that simplify the analysis over that for sources such as Sgr B2, which is also quite rich but suffers from non-Gaussian, broad line profiles as a result of outflows. Thus, G327 provides an excellent "standard source" with which chemical models may be compared. Chemically, G327 is a good source for which to do molecule searches for these reasons as well. When a southern hemisphere millimeter array, such as the Atacama Large Millimeter Array, is completed, it would be instructive to map G327 on a subarcsecond level. By doing this we could test for such things as a sudden jump in methanol abundance at close proximity to the hot core, which would help pin down the icy grain mantle contribution. Also, more detailed data could give a better handle on those molecules for which a multicomponent model of the source chemistry may best describe a population (CH_3OH, CH_3OCH_3, CH_3OCHO) but for which analysis of our data with a 20″ or larger beam was inadequate.

The authors gratefully acknowledge financial support from NASA under grant NAG5-7598 (E. G., A. N., and D. C. B. W.), NAG5-8718 (W. M. I.), and the Swedish Natural Science Research Council, NFR (P. B.). We would like to thank the SEST staff for friendly and professional help with observations during our many observing runs. We would also like to thank J. E. Dickens, M. Ikeda, and M. Ohishi for making some of the observations, Å. Hjalmarson and L. E. Snyder for helpful comments in the preparation of this manuscript, and J. C. Pearson for providing frequencies for vibrationally excited ethyl cyanide lines prior to publication. We also thank S. Charnley for his helpful comments on this manuscript.

REFERENCES

Anderson, T., De Lucia, F. C., & Herbst, E. 1990, ApJS, 72, 797
Anderson, T., Herbst, E., & De Lucia, F. C. 1987, ApJS, 64, 703
Bachiller, R., Liechti, S., Walmsley, C. M., & Colomer, F. 1995, A&A, 295, L51
Bergman, P. 1992, Ph.D. thesis, Chalmers Univ. Technology (Tech. Rep. 277)
Bernstein, M. P., Sandford, S. A., & Allamandola, L. J. 1997, ApJ, 476, 932
Bernstein, M. P., Sandford, S. A., Allamandola, L. J., Chang, S., & Scharberg, M. A. 1995, ApJ, 454, 327
Bettens, F. L., Sastry, K. V. L. N., Herbst, E., Albert, S., Oesterling, L. C., & De Lucia, F. C. 1999, ApJ, 510, 789
Blake, G. A., Sutton, E. C., Masson, C. R., & Phillips, T. R. 1987, ApJ, 315, 621
Booth, R. S., et al. 1989, A&A, 216, 315
Caselli, P., Hasegawa, T. I., & Herbst, E. 1993, ApJ, 408, 548
Cernicharo, J., et al. 1999, in The Universe as Seen by *ISO*, ed. P. Cox & M. F. Kessler (ESA-SP 427; Paris: UNESCO), 565
Cesaroni, R., Walmsley, C. M., & Churchwell, E. 1992, A&A, 256, 618
Charnley, S. B. 1997, ApJ, 481, 396
Charnley, S. B., Kress, M. E., Tielens, A. G. G. M., & Millar, T. J. 1995, ApJ, 448, 232
Charnley, S. B., Tielens, A. G. G. M., & Millar, T. J. 1992, ApJ, 399, L71
Cragg, D. M., Johns, K. P., Godfrey, P. D., & Brown, R. D. 1992, MNRAS, 259, 203
Dartois, E., Schutte, W., Geballe, T. R., Demyk, K., Ehrenfreund, P., & d'Hendecourt, L. 1999, A&A, 342, L32
Dickens, J., Irvine, W. M., Nummelin, A., Gibb, E., Hjalmarson, Å., Ohishi, M., & Saito, S. 2000, Spectrochim. Acta, submitted
Ehrenfreund, P., Dartois, E., Demyk, K., & d'Hendecourt, L. 1998, A&A, 339, L17
Ehrenfreund, P., van Dishoeck, E. F., Burgdorf, M., Cami, J., van Hoof, P., Tielens, A. G. G. M., Schutte, W. A., & Thi, W. F. 1997, Ap&SS, 255, 83
Gensheimer, P. D., Mauersberger, R., & Wilson, T. L. 1996, A&A, 314, 281
Gezari, D. Y., Schmitz, M., & Mead, J. M. 1987, Catalog of Infrared Observations (NASA Ref. Publ. 1196)
Gibb, E. L., et al. 2000, ApJ, 536, 347
Goldsmith, P. F., & Langer, W. D. 1999, ApJ, 517, 209
Gomez, Y., Rodriguez, L. F., Garay, G., & Moran, J. M. 1991, ApJ, 377, 519
Groner, P., Albert, S., Herbst, E., & De Lucia, F. C. 1998, ApJ, 500, 1059
Hatchell, J., Thompson, M. A., Millar, T. J., & Macdonald, G. H. 1998, A&AS, 133, 29

Helmich, F. P., & van Dishoeck, E. F. 1997, A&AS, 124, 205
Irvine, W. M., Ohishi, M., & Kaifu, N. 1991, Icarus, 91, 2
Kuan, Y. J., & Snyder, L. E. 1996, ApJ, 470, 981
Kutner, M. L., & Ulich, B. L. 1981, ApJ, 250, 341
Lacy, J. H., Faraji, H., Sandford, S. A., & Allamandola, L. J. 1998, ApJ, 501, L105
Lampton, M., Margon, B., & Bowyer, S. 1976, ApJ, 208, 177
Linke, R. A., Frerking, M. A., & Thaddeus, P. 1979, ApJ, 234, L139
Liu, S. Y., & Snyder, L. E. 1999, ApJ, 523, 683
Lovas, F. J. 1984, Spectral Line Atlas of Interstellar Molecules (Gaithersburg: National Inst. Standards and Technology)
Lovas, F. J. 1985, J. Phys. Chem. Ref. Data, 14, 395
Macdonald, G. H., Gibb, A. G., Habing, R. J., & Millar, T. J. 1996, A&AS, 119, 333
Millar, T. J., Macdonald, G. H., & Gibb, A. G. 1997, A&A, 325, 1163
Minh, Y. C., Ohishi, M., Roh, D. G., Ishiguro, M., & Irvine, W. M. 1993, ApJ, 411, 773
Nummelin, A., & Bergman, P. 1999, A&A, 341, L59
Nummelin, A., Bergman, P., Hjalmarson, Å., Friberg, P., Irvine, W. M., Millar, T. J., Ohishi, M., & Saito, S. 1998a, ApJS, 117, 427
———. 2000, ApJS, 128, 213
Nummelin, A., Dickens, J. E., Bergman, P., Hjalmarson, Å, Irvine, W. M., Ikeda, M., & Ohishi, M. 1998b, A&A, 337, 275
Oesterling, L. C., Albert, S., De Lucia, F. C., Sastry, K. V. L. N., & Herbst, E. 1999, ApJ, 521, 255
Palumbo, M. E., Tielens, A. G. G. M., & Tokunaga, A. T. 1995, ApJ, 449, 674
Pendleton, Y. J., Tielens, A. G. G. M., Tokunaga, A. T., & Bernstein, M. P. 1999, ApJ, 513, 294
Pickett, H. M., Poynter, R. L., Cohen, E. A., Delitsky, M. L., Pearson, J. C., & Muller, H. S. P. 1998, J. Quant. Spectrosc. Radiat. Transfer, 60, 883
Sandford, S. A., Allamandola, L. J., & Bernstein, M. P. 1997, in ASP Conf. Ser. 122, From Stardust to Planetesimals, ed. Y. J. Pendleton & A. G. G. M. Tielens (San Francisco: ASP), 201
Schilke, P., Groesbeck, T. D., Blake, G. A., & Phillips T. G. 1997, ApJS, 108, 301
Schilke, P., Phillips, T. G., & Mehringer, D. M. 1999, in The Physics and Chemistry of the Interstellar Medium, ed. V. Ossenkopf, J. Stutzki, & G. Winnewisser (Herdecke: GCA-Verlag)
Schmidt-Kaler, Th. 1982, The Physical Parameters of the Star, in Landolt-Börnstein New Series, Group IV, Vol. 2b, ed. K. Schaifers & H. H. Voigt (New York: Springer), 1
Schutte, W. A., & Greenberg, J. M. 1997, A&A, 317, L43
Simpson, J. P., & Rubin, R. H. 1990, ApJ, 354, 165
Sobolev, A. M., Cragg, D. M., & Godfrey, P. D. 1997, MNRAS, 288, L39
Sutton, E. C., Peng, R., Danchi, W. C., Jaminet, P. A., Sandell, G., & Russel, A. P. G. 1995, ApJS, 97, 455
Taylor, S. D., Morata, O., & Williams, D. A. 1998, A&A, 336, 309
Thompson, M. A., & Macdonald, G. H. 1999, A&AS, 135, 531
Tielens, A. G. G. M., & Charnley, S. B. 1997, Origins Life & Evol. Biosphere, 27, 23
Turner, B. E. 1991, ApJS, 76, 617
van Dishoeck, E. F., & Blake, G. A. 1998, ARA&A, 36, 317
Wegner, W. 1994, MNRAS, 270, 229
Whittet, D. C. B. 1992, Dust in the Galactic Environment (Bristol: IOP)
Wilson, T. L., & Rood, R. T. 1994, ARA&A, 32, 191
Wood, D. O. S., & Churchwell, E. 1989, ApJS, 69, 831
Wyrowski, F., Schilke, P., & Walmsley, C. M. 1999, A&A, 341, 882